Intestinal microbiota programming of alveolar macrophages influences severity of respiratory viral infection

Vu L. Ngo[1#], Carolin M. Lieber[1#], Hae-ji Kang[1], Kaori Sakamoto[2], Michal Kuczma[1], Richard K. Plemper[1&*], and Andrew T. Gewirtz[1&*]

Affiliation:

1. Center for Translational Antiviral Research, Georgia State University Institute for Biomedical Sciences, Atlanta GA 30303, USA.

2. Department of Pathology, University of Georgia College of Veterinary Science, Athens GA 30602, USA

# These authors contributed equally to this work

& Denotes co-senior authors

*Corresponding authors. Email: rplemper@gsu.edu
agewirtz@gsu.edu

Abstract (132 words)

Investigating the influence of intestinal microbiota composition on respiratory viral infection (RVI) revealed that segmented filamentous bacteria (SFB), naturally acquired or exogenously administered, protected mice against influenza virus (IAV) infection, as assessed by viral titers, histopathology, and clinical disease features. Such protection, which also applied to RSV and SARS-CoV-2, was independent of interferon and adaptive immunity but required basally resident alveolar macrophages (AM), which, in SFB-negative mice, were quickly depleted as RVI progressed. Examination of AM from SFB-colonized mice revealed that they were intrinsically altered to resist IAV-induced depletion and inflammatory signaling. Yet, AM from SFB-colonized mice were not quiescent. Rather, they directly disabled IAV via enhanced complement production and phagocytosis. Transplant of SFB-transformed AM into SFB-free hosts recapitulated SFB-mediated protection against IAV mechanistically linking intestinal microbiota, AM phenotype, and RVI severity.

One sentence summary: Intestinal segmented filamentous bacteria reprogram alveolar macrophages enabling their host to withstand respiratory viruses.

41 **INTRODUCTION**

42 Outcomes following exposure to respiratory viruses, such influenza A viruses (IAV),
43 respiratory syncytial virus (RSV), and SARS-CoV-2, vary widely amongst individuals, ranging
44 from asymptomatic infection to severe lung pathology and/or death. While determinants of such
45 heterogeneity to respiratory viral infection (RVI) are likely numerous and complex, we
46 hypothesized that one important factor is gut microbiota composition [1], which is now
47 appreciated to have broad influence over a range of chronic inflammatory diseases and the
48 immune responses with which such diseases are associated [2]. For example, studies comparing
49 mice captured in the wild to those bred for generations in well-controlled vivaria revealed vast
50 differences in their microbiomes that resulted in wild mice having highly and broadly activated
51 immune systems and being relatively resistant to IAV [3, 4]. Yet, differences in specific
52 microbial species that can impact RVI outcomes, and how they might do so, have not been well
53 defined. Hence, we studied mice raised in vivaria with discrete defined microbiome differences
54 and, subsequently, mice differing in only the presence or absence of a single common species,
55 namely segmented filamentous bacteria (SFB). We found that gut SFB dictated the phenotype of
56 alveolar macrophages and, consequently, outcomes of RVI.

57

58

59 **RESULTS**

60

61 ***SFB protects mice from IAV infection***

62 Appreciation of the potential of microbiota to broadly impact health led one commercial
63 rodent supplier to offer "excluded flora (EF)" mice, which were bred in a restricted vivarium that
64 assured absence of a discrete panel of disease-modulating commensal microbes, which might or
65 might not otherwise be present in colonies of "specific pathogen-free (SPF)" mice commonly
66 used in biomedical research [5]. We used such mice as a starting point to probe the influence of
67 microbiota composition on RVI. Specifically, we compared proneness of SPF and EF mice to
68 IAV infection 4 days following intranasal administration of 2009 pandemic A/CA/07/2009
69 (H1N1), herein referred to as CA09, which readily infects mice without need for species
70 adaptation and recapitulates major clinical features of human disease in the animal model [6].
71 Compared to EF mice, SPF mice exhibited significantly reduced lung viral titers. Furthermore,
72 SPF mice did not show hypothermia and weight loss observed in EF mice **(Figure 1A)**.
73 Additionally, although not designed as a survival experiment per se, we noted that some mice of
74 the EF mice required euthanasia. These results suggested that one or more of the microbes
75 specifically excluded from EF mice might confer protection against IAV.

76 Of the panel of organisms known to be absent in EF mice, segmented filamentous
77 bacteria (SFB) stood out as a potential modulator of IAV proneness in that SFB, despite being a
78 strict anaerobe and, thus, restricted to the intestinal luminal surface, is known to systemically
79 impact T-lymphocytes [7, 8]. Furthermore, SFB is a major contributor to, albeit not the sole
80 mediator of, the spontaneous resistance to rotavirus (RV), an intestinal pathogen, that
81 spontaneously arose in some mouse colonies [9]. SFB is very challenging to culture but can be

82 isolated, maintained, and studied by administering it via fecal microbial transplantation (FMT).
83 Hence, mice lacking SFB but otherwise carrying a complex SPF microbiota, herein referred to as
84 SFB^- mice, were administered a FMT from other SFB^- mice, mice containing SFB as one natural
85 component of their SPF microbiota, or germ-free mice that had been monoassociated (MA) with
86 SFB. Such mice were inoculated with CA09 one-week post-FMT and euthanized 4d later to
87 measure lung viral titers or monitored for 14 days to assess clinical-type disease parameters.
88 Mice receiving FMT from mice naturally colonized with SFB exhibited IAV titer reductions of
89 approximately one order of magnitude compared to animals that lacked SFB and, concomitantly,
90 clinical signs of IAV infection were ameliorated **(Figure 1B).** FMT from SFB-MA mice fully
91 recapitulated such protection while administering feces from germ-free mice was without effect
92 (**Figure S1A).** Thus, administering SFB^- mice a FMT from SFB-MA mice, hereafter referred to
93 as administering SFB, recapitulated the differential proneness of EF and SPF mice to IAV
94 infection, thus providing a tractable model to investigate how the presence of this specific gut
95 microbiota constituent, within a complex microbial ecosystem, reduced IAV infection in the
96 lung.
97 SFB-mediated protection against IAV infection was evident, albeit seemingly not
98 maximal, two days post SFB administration and was undiminished three months later (longest
99 time tested) despite gut SFB levels having declined by over 60-fold from peak to a stable plateau
100 by this time **(Figure 1C and Figure S1B).** In accord with its relative abundance not being a
101 critical variable, SFB colonized 24-week-old mice at 10-fold lower levels than 5-week-old mice
102 but still protected them against IAV infection **(Figure S1C)**. Consistent with previous
103 observations that SFB only resides in the gut lumen or attached to the apical epithelial gut
104 surface [10], SFB was readily detected by PCR in the ileum, but was not found in the lung or

spleen **(Figure 1D)**. Histopathologic examination of lung tissue did not detect any impact of SFB itself on the lung but revealed a striking suppression of IAV-induced lung pathology **(Figure 1E)**. Such protection of lung tissue was potentially attributable to the one-log reduction in observed in viral tiers conferred by SFB colonization but also hinted at the possibility that SFB had reduced IAV-induced inflammatory signaling.

SFB's protection against IAV not explained by known candidate mechanisms

SFB-mediated lasting protection against IAV contrasted with its transient protection against RV [9], suggesting that the former might be mediated by adaptive immunity. However, SFB-mediated protection against IAV was fully maintained in *Rag1*$^{-/-}$ mice, which lack most T and B lymphocytes, arguing against this notion **(Figure 2A)**. Innate antiviral immunity typically involves interferon and can involve innate lymphoid cells (ILC) and/or IL-22 and IL-17. Yet, SFB-mediated protection against IAV was maintained in *Ifnar*$^{-/-}$ mice, which lack type I interferon signaling, *Rag1*$^{-/-}$-*Il2rg*$^{-/-}$, which lack type 3 ILC, and upon antibody-mediated neutralization of IL-17 and IL-22 **(Figure 2B-D)**. SFB-mediated protection against IAV was also maintained in *Stat1*$^{-/-}$ animals, which are broadly compromised in IFN signaling **(Figure 2E)**. These results argue against a role for any of these candidate host mechanisms in mediating SFB's protection against IAV infection. We also considered a candidate microbial mechanism. Specifically, we hypothesized that the protection against IAV conferred by SFB might reflect that it induced an array of complex changes in other taxa that might then broadly impact innate immunity. However, SFB's protection was maintained in Altered Schaedler flora (ASF) mice, which harbor only a minimal 8-species microbial community [11] thus arguing against this possibility.

128

129 ***SFB's protection against IAV, RSV and SARS-CoV-2 associated with preservation of resident***
130 ***lung phagocytes***

131 That candidate mechanisms were not experimentally substantiated led us to utilize less
132 targeted approaches to investigate how SFB gut colonization protected mice against IAV. First,
133 we performed transcriptomic profiling of whole lungs harvested from mice thar were untreated
134 (naïve) or administered SFB, CA09, or a combination thereof. The results of this RNA-seq
135 analysis were presented as a heat map, showing 4-5 individual mice per condition, of all genes
136 whose expression was significantly altered in response to any of the three treatments **(Figure**
137 **3A)**. It illustrated that SFB, by itself, had almost no impact on lung gene expression, whereas, as
138 expected, IAV infection, by itself, markedly remodeled the lung transcriptome. Strikingly, such
139 IAV-induced changes in gene expression were absent in SFB-colonized mice, indicating that the
140 presence of SFB in the gut broadly ameliorated IAV's impact on lung tissue. The majority of
141 genes induced by CA09-induced were related to immunity and inflammation thus according with
142 the view that much of the lung pathology in IAV infection is driven by the immune system [12]
143 and, furthermore, the notion that SFB strongly dampened such responses.

144 We next used flow cytometry to examine the impact of SFB and IAV on lung populations
145 of immune cells, focusing on innate cells given our results from KO mice had suggested
146 lymphocytes were not required SFB-mediated protection against IAV. Consistent with other
147 studies, intranasal administration of CA09, by itself, induced a stark depletion of basally-resident
148 $CD103^{+}$ dendritic cells (cDC1) and alveolar macrophages (AM), which was followed by
149 increased abundance of a panel of inflammatory cells including neutrophils, monocytes, and
150 natural killer cells [13]. Analogous to the RNA-seq and histopathology results, SFB, by itself,

151 did not significantly impact levels of lung leukocytes but wholly prevented the changes induced
152 by CA09 **(Figure 3B and Figure S2)**. Preventing these CA09-induced changes in lung
153 cellularity and disease was not SFB strain-specific as similar protective effects resulted from
154 colonization of the gut by SFB strains isolated in 3 different continents **(Figure S3)**. Nor were
155 SFB impacts specific to IAV. Rather, SFB colonization also reduced viral loads and prevented
156 changes in lung cellularity, and reduced pro-inflammatory gene expression, following
157 inoculation of mice with respiratory syncytial virus (RSV) and mouse-adapted SARS-CoV-2
158 **(Figure S4)**. which, irrespective of SFB, did not cause clinical signs of disease.
159 To investigate the extent to which SFB-mediated prevention of IAV-induced changes in
160 lung cellularity simply reflected lower IAV loads, we pharmacologically restricted IAV
161 replication via 4'-fluorouridine (4'-FIU), a broad-spectrum nucleoside analog inhibitor that we
162 recently reported impedes IAV, RSV, and SARS-CoV-2 [14, 15]. SFB^- mice received 4'-FIU via
163 oral gavage at different dose levels in a once daily (q.d.) regimen beginning 24 hours post-
164 inoculation. At this time, IAV levels and immune cell populations were similar in SFB^- and SFB-
165 administered mice **(Figure S2C)**, which we hereafter refer to as SFB^+ mice. As expected,
166 administration of 4'-FIU to SFB^- mice dose-dependently suppressed IAV replication to a similar
167 or greater extent than SFB **(Figure 3C)**. Like SFB, 4'-FIU administration prevented the CA09-
168 induced appearance of inflammatory cells in the lung. However, even the highest dose of 4'-FIU,
169 which lowered IAV titers by over three orders of magnitude, did not mitigate CA09-induced
170 ablation of cDC1 or AM suggesting that their persistence in SFB^+ mice may have contributed to,
171 rather than resulted from, suppression of IAV.
172
173 ***Alveolar Macrophages are required for SFB-mediated protection against IAV***

174 Potential roles for cDC1 and AM in SFB-mediated protection against IAV were tested in
175 mice harboring deficiencies in these cells. We observed that SFB-mediated protection against
176 IAV was maintained in *Batf3*$^{-/-}$ mice, which wholly lack cDC1 [16], but was greatly reduced in
177 *Csf2*$^{-/-}$ mice, which have a 70% reduction in basal AM levels [17] **(Figure 4 A&B)**. The role of
178 AM was further examined by depleting these cells with clodronate liposomes [18], an approach
179 that we verified efficiently depleted AM but did not alter levels of other lung innate immune
180 cells **(Figure 4Ci)**. Depletion of AM, by itself, did not significantly impact IAV titers or clinical
181 signs of disease but eliminated the ability of SFB to lower lung IAV titers, ameliorate
182 hypothermia and weight loss, and prevent death **(Figure 4Cii)**. These results suggested that SFB-
183 mediated impacts on AM were germane to its protection against RVI. SFB-mediated
184 maintenance of AM levels could conceivably have reflected increased generation of these cells,
185 which can occur from monocyte progenitors migrating to the lung or local self-renewal [19], or
186 that SFB colonization had resulted in AM resisting death upon RVI. SFB's prevention of AM
187 depletion following CA09 inoculation associated with prevention of IAV-induced caspase-3
188 activation **(Figure 4D)**, which marks AM commitment to cell death [20], and increased
189 expression of CD71 **(Figure 4E)**, which associates with enhanced phagocytosis and survival [21,
190 22]. These results suggest that SFB colonization had "emboldened" AM to resist IAV-induced
191 depletion.
192
193 ***SFB's preservation of AM enables their sustained protection of EC from IAV infection***
194 Airway epithelial cells (AEC) are primary sites replication sites of respiratory viruses,
195 including IAV, RSV, and SARS-CoV-2. Specifically, in the case of highly pathogenic H1N1
196 IAV, AEC are the only site in which hemagglutinin is effectively cleaved to allow infection,

197 replication, and generation of new infectious virions [23]. AM are known to protect lung airway
198 epithelial cells (AEC) from IAV infection, particularly at early time points following IAV-
199 infection, i.e. prior to their depletion [24]. Thus, we predicted that SFB's preservation of AM
200 following CA09 inoculation might result in lower viral loads in AEC in SFB^+ mice. Indeed, the
201 percentage of lung AEC, type I and II, as well as conducting AECs, displaying detectable levels
202 of CA09, which encodes GFP, by flow cytometry, was significantly reduced in SFB^+ mice 4
203 days post-inoculation **(Figure 4E and Figure S5)**. Depletion of AM by clodronate in SFB^+ mice
204 increased IAV levels to that of SFB^- mice in all three lung AEC types **(Figure 4F)**. These results
205 indicate that SFB-induced AM persistence following IAV infection enables sustained AM-
206 mediated protection of EC, likely contributing to lower IAV burden and ameliorated pathology.
207
208 ***Persistence of SFB^+ AM upon RVI is cell-intrinsic***
209 Persistence of AM in CA09-infected SFB^+ mice was potentially attributable to SFB
210 altering the lung environment and/or reflect that AM themselves had been intrinsically
211 transformed to better withstand IAV challenge. To differentiate between these possibilities, we
212 adoptively transferred FACS-sorted AM from SFB^+ and SFB^- mice to SFB^- mice using donor
213 mice with a CD45.1 subtype, thereby enabling distinction of endogenous and transplanted cells
214 **(Figure 5)**. The degree to which AM harvested from SFB^+ and SFB^- mice, hereafter referred to
215 as SFB^+ and SFB^- AM, engrafted following transplant was similar, comprising about 20% of the
216 total AM in their new host. CA09 infection did not significantly alter proportions of endogenous
217 vs. engrafted AM in recipients of SFB^- AM but led to SFB^+ AM (i.e. engrafted) becoming their
218 host's majority AM population. This shift in AM proportions reflected that endogenous AM in
219 both recipient groups as well as engrafted SFB^- AM were all depleted by CA09 infection,

220 whereas engrafted SFB$^+$ AM fully resisted CA09-induced depletion and, concomitantly, lacked
221 Caspse-3 activation, despite having been transplanted into an SFB-free host. Thus, colonization
222 of the gut with SFB intrinsically altered AM to withstand IAV-induced depletion.
223
224 ***SFB$^+$ AM exhibited inflammatory anergy and enhanced antiviral function***
225 Differences between SFB$^+$ and SFB$^-$ AM were characterized ex vivo as schematized
226 **(Figure 6A).** Profiling of basal gene expression (i.e. without IAV exposure) by RNA-seq found
227 that only 24 of the 15,510 genes expressed by AM were differentially expressed between SFB$^-$
228 and SFB$^+$ AM **(Figure 6B)**, 18 of which were both confirmed by PCR and biologically
229 replicated in a distinct mouse cohort **(Figure S6A).** Six of the genes upregulated in SFB$^+$ AM are
230 associated with an M2 macrophage phenotype. Yet, quantitation of surface expression markers
231 previously used to distinguish M1 vs. M2 phenotypes [25] did not reveal differences between
232 SFB$^+$ and SFB$^-$ AM **(Figure S6B)**. The genes most prominently up- and down-regulated,
233 respectively, in SFB$^+$ AM were Tsc22d3 and Notch 4, which, respectively, function in
234 suppressing and activating pro-inflammatory gene expression [26, 27] suggesting such signaling
235 might be dampened in SFB$^+$ AM. Indeed, we found SFB$^+$ AM lacked the robust UV-irradiated
236 IAV-induced activation of pro-inflammatory gene expression exhibited by SFB$^-$ AM **(Figure 6C**
237 **and Figure S7A)**. Such lack of pro-inflammatory responsiveness was partially recapitulated by
238 antibody-mediated neutralization of Notch 4 suggesting that the reduced Notch 4 expression in
239 SFB$^+$ AM contributed to their inflammatory anergy and, consequently, the reduced inflammation
240 observed in IAV-infected SFB$^+$ mice.
241 The small panel of genes upregulated in SFB$^+$ AM also included those known to function
242 in antiviral resistance, including complement C1qa and Ifitm1 thus suggesting that SFB$^+$ AM

243 were not anergic to IAV per se but, rather, might have better virus neutralizing capacity. We
244 examined this possibility by incubating CA09 stocks with AM for 45 min at which time AM
245 were removed by centrifugation and supernatant infectious titers and IAV genomes quantified.
246 SFB^- AM lowered the infectious titers of the CA09 stocks to which they were exposed, at 37ºC
247 but not 4ºC, but the extent of reduction was 150-fold greater for SFB^+ AM (**Figure 6Di**). This
248 greater reduction in titer was accompanied by only 5-fold lower levels of PCR-quantifiable IAV
249 genomes in supernatants of SFB^+ AM (**Figure 6Dii**). This led us to hypothesize enhanced
250 neutralization of IAV by complement and/or other products secreted by SFB^+ AM. Indeed, we
251 found that, even when SFB^+ AM were not exposed to virus, their supernatants from 18h cultures
252 had greater capacity than those from SFB^- AM to lower CA09 infectious titers **(Figure 6Diii**).
253 Such enhanced ability of SFB^+ AM supernatants to lower IAV titers was fully reversed by
254 antibody-mediated removal of C1qa and, moreover, was not observed in $C1qa^{-/-}$ mice **(Figure**
255 **S6C)**. These results accord with recent observations that C1qa can directly bind IAV and reduce
256 its infectivity [28]. Yet, in contrast to AM themselves, addition of AM supernatants to CA09
257 stocks had no impact on levels of viral genomes (**Figure S6D**) suggesting the enhanced antiviral
258 capacity of SFB^+ AM might also involve increased viral absorption and/or uptake, potentially as
259 a result of viral particles being more decorated with C1qa [29]. In accord with this notion,
260 reductions in IAV genomes in supernatants of AM/CA09 mixtures were paralleled by increased
261 IAV genomes in AM lysates **(Figure 6Div**). The relative increase in IAV genomes in SFB^+,
262 compared to SFB^-, AM lysates was maintained amidst chlorpromazine, but not latrunculin
263 treatment, neither of which impacted cell viability, suggesting it might reflect enhanced
264 phagocytosis uptake by SFB^+ AM (**Figure S6F**). In accord with this notion, SFB^+ AM exhibited
265 modestly greater uptake of IgG-coated fluorescent beads **(Figure S6E**). Exploring the fate of

266 CA09 internalized by AM during the 45 min exposure period found that, 24 h following media
267 replacement, AM supernatants had few infectious virions while lysates contained few detectable
268 IAV genomes **(Figure 6Div**) thus suggesting that AMs were not permissive for CA09
269 replication, but rather constituted a dead end for the virus. Collectively, these results indicate that
270 elevated C1qa expression and, perhaps consequently, enhanced phagocytosis drove the increased
271 antiviral capacity of SFB^+ AM.
272
273 ***SFB-induced reprogramming of AM protects mice against IAV infection***
274 Lastly, we examined the extent to which SFB-induced reprogramming of AM contributed
275 to SFB's protection against IAV infection. Specifically, we performed an additional series of
276 AM transplant experiments designed to measure impacts on IAV levels and clinical-type
277 parameters. Consistent with the notion that AM, prior to their depletion, protect against IAV
278 infection [24], we observed that administration of SFB^- AM to a host replete with endogenous
279 AM resulted in a modest reduction in IAV titers, gross lung damage, hypothermia, weight loss,
280 and death following CA09 inoculation **(Figure 7A)**. Administration of SFB^+ AM provided
281 markedly greater protection against this IAV challenge, approximating the level conferred by
282 administration of SFB itself, as assessed by all parameters measured. Analogous patterns of
283 results were seen following transfer of SFB^+ and SFB^- AM into mice deficient in endogenous
284 AM, achieved via use of *Csf2*$^{-/-}$ mice or chlodronate administration **(Figure 7B and 7C)**. *Ex vivo*
285 blockade of Notch4 on SFB^- AM prior to transplanting them also enhanced their ability to
286 withstand IAV-induced depletion, protect EC from IAV infection, and ameliorate CA09-induced
287 disease, but did not impact level of viral genomes in the lung **(Figure S7B)**, suggesting the
288 ability of transplanted SFB^+ AM to do so was not mediated solely by dampened inflammatory

289 signaling but also required such AM have enhanced antiviral function. Thus, SFB colonization of
290 the gut stably and broadly altered the AM phenotype enabling these cells to better protect their
291 hosts from lethal RVI.
292
293
294

295 **DISCUSSION**

296 Positioned in the lung lumen to enable their guarding the surfaces of 0_2 and CO_2
297 exchange, AM are amongst the first cells to encounter inhaled threats including respiratory
298 viruses. We show herein that how AM respond to respiratory viruses is dramatically altered by
299 the composition of the intestinal microbiota. Specifically, we report that colonization of the
300 intestine by SFB, naturally acquired, or exogenously administered, markedly attenuates IAV-
301 induced AM pro-inflammatory gene expression while increasing ability of AM to directly
302 disable IAV. SFB-induced reprogramming of AM manifested in vivo by them resisting RVI-
303 induced depletion thereby enabling their sustained protection of lung epithelial cells from
304 infection. Collectively, these consequences of SFB-induced AM reprogramming resulted in
305 lower viral titers, reduced inflammation and, consequently, reduced disease severity. While the
306 general concept that microbiota composition in total can influence immune phenotype and,
307 proneness to infection is established [30, 31], we were quite surprised that the presence of a
308 single common commensal bacterial species, amidst the thousands of different microbial species
309 that variably inhabit the mouse gut, had such strong impacts in RVI models and, furthermore,
310 that such impacts were largely attributable to reprogramming of AM.

311 The extent to which SFB is present in humans is not well defined but it has been reported
312 to be frequently present in children in some regions [32] and was unequivocally shown to be
313 present in some adult individuals [33]. Yet independent of a specific role for SFB, however, our
314 findings speak strongly to the potential of gut microbiota to influence proneness to RVI,
315 especially via programming of AM. Both AM pro-inflammatory gene expression and AM
316 depletion are known to correlate with RVI severity in humans but determinants of inter-
317 individual heterogeneity in AM responses have not been defined [32]. We consider it highly

318 unlikely that SFB is the only gut microbe capable of impacting AM phenotype and,
319 consequently, proneness to RVI. Rather, we posit that AM are a key component of the gut-lung
320 axis wherein an individual's microbiota in its entirety is a determinant of disease outcome
321 following exposure to an array of respiratory viruses.

322 The observation that SFB^+ AM maintained an IAV-resistant phenotype following
323 transplant to SFB^- mice is consistent with observations that AM have stable cell-type specific
324 patterns of gene expression and methylation even when cultured extensively *ex vivo* [34].
325 Moreover, it accords with recently increasing appreciation that AM can be "entrained" to display
326 long-lasting phenotypic alterations that impact their ability to manage pathogens and tumors
327 [35]. Yet, mechanisms governing such AM entraining are not clear and, moreover, may be
328 distinct from the AM reprogramming observed here. Specifically, previously observed AM
329 entraining has generally involved large-scale depletion of AM, which are then replaced by cells
330 newly recruited from bone marrow that, even after establishing residency in the lung, exhibit
331 stark global differences in gene expression profiles. In contrast gene expression profiling of SFB^-
332 and SFB^+ AM revealed only modest differences, likely reflecting that both AM had been
333 generated by AM self-renewal processes that normally maintain AM homeostasis in non-
334 traumatic states. Nonetheless, changes in basal AM gene expression we observed likely
335 contributed to the enhanced ability of SFB^+ AM to protect their host against RVI. Indeed, the
336 inflammatory anergy, mediated in part by reduced Notch-4 expression, and enhanced antiviral
337 function, mediated in part by elevated C1qa expression, of SFB^+ AM plausibly directly
338 contributed to, respectively, the reductions in lung pathology and viral loads that followed IAV
339 inoculation. Much less clear, and thus warranting further research, is the nature of the signal that

340 is generated by SFB colonization of the luminal surface of the intestine that drives AM
341 reprogramming.
342 In addition to directly disabling IAV, AM can also protect lung EC from IAV infection
343 via suppressing EC CysLT1 signaling, which might mediate IAV entry into these cells [24].
344 Thus, persistence of AM in SFB^+ mice, by itself, likely contributed to SFB's protection against
345 IAV. That mechanisms driving RVI-induced AM depletion are not clear, makes determining
346 how SFB colonization prevents such depletion challenging. Nonetheless, we speculate that
347 reductions in inflammatory gene expression and viral loads, which SFB+ AM mediated, may
348 have contributed to increased persistence of SFB^+ AM. In addition to mitigating primary RVI,
349 AM persistence may help prevent secondary consequences of RVI. Many of the severe
350 consequences of IAV infection in humans result from secondary bacterial infections, to which
351 the lung is made more permissive by loss of IAV-induced AM depletion [36]. Such impaired
352 antibacterial immunity can persist for prolonged periods perhaps reflecting that the bone-marrow
353 derived replacement AM are not quickly optimized for mucosal host defense. Thus, microbiota
354 mediated AM programming may not only influence severity of acute RVI but may also be a long
355 term post-RVI health determinant.
356

MATERIALS AND METHODS

Mice

The following mice were purchased from The Jackson Laboratory: C57BL/6 (B6 WT), B6.129S(C)-*Batf3*^{tm1Kmm}/J, B6.129S-*Csf2*^{tm1Mlg}/J, B6.129S7-*Rag1*^{tm1Mom}/J, B6.129S2-*Ifnar1*^{tm1Agt}/Mmjax, NOD.Cg-*Rag1*^{tm1Mom} *Il2rg*^{tm1Wjl}/SzJ, B6.129S(Cg)-*Stat1*^{tm1Dlv}/J, B6(Cg)-C1qatm1d(EUCOMM)Wtsi/TennJ. The Jackson laboratory does not test mice for the presence of segmented filamentous bacteria (SFB), but all mice we tested that were purchased from this provider for this study were SFB-negative upon arrival at GSU. The following mice were purchased from Taconic Biosciences: C57BL/6 (B6 WT) Excluded Flora (EF) mice and Specific Pathogen-Free (SFP) mice, which we verified were SFB$^+$ and SFB$^-$, respectively. Unless otherwise stated, mice were used at 4-5 weeks of age, and experiments were carried out using age- and gender-matched groups. The Institutional Animal Care and Use Committee of Georgia State University approved animal studies.

PCR primers, FACs antibodies, neutralization antibodies and other reagents

All reagents used in these manuscripts can be seen in Tables S1 and S2.

Cells and viruses

Madin-Darby Canine Kidney (MDCK; ATCC CCL-34), HEp-2 (ATCC CCL-23), and VeroE6 TMPRSS2 (BPS Bioscience #78081) cells were cultured in Dulbecco's Modified Eagle's Medium (DMEM) supplemented with 7.5% heat-inactivated fetal bovine serum (FBS) at 37°C and 5% CO_2. All cell lines used in this study were authenticated and checked for *Mycoplasma* and microbial contamination. Recombinant Influenza A virus was recovered based on original

380 reports for laboratory-adapted IAV [37]. A/CA/07/2009 (H1N1) was grown on MDCK cells
381 using serum-free DMEM supplemented with 0.5% Trypsin. Recombinant RSV strain A2 with
382 line19F reporter gene recRSV-mKate was rescued and amplified as described previously [38],
383 and the SARS-CoV-2 MA10 strain [39] was passaged in VeroE6 TMPRSS2 cells. All viruses
384 used were clarified, aliquoted, and stored at -80°C. Virus stock titers were determined through
385 $TCID_{50}$-titration.
386

387 **Complex microbiota and mono-associated SFB transplantation**

388 Fecal samples were collected from donor mice, suspended in 20% glycerol PBS solution at 40
389 mg/mL concentration, passed through a 40 µm filter, and stored at -80C. Frozen fecal
390 suspensions were orally administered to recipient mice at 200 µl per mouse.
391

392 **Virus infection**

393 Unless otherwise stated, mice were 5 weeks of age at the time of infection. Mice were randomly
394 assigned to study groups and housed under ABSL-2 or ABSL-3 conditions for infections with
395 A/CA/07/2009 (H1N1) recombinant, recRSV-mKate, or SARS-CoV-2 MA10 strain,
396 respectively. Seven days prior to virus infection, mice were subjected to microbiota manipulation
397 (administration of feces from SPF or SFB-monoassociated mice). Bodyweight was determined
398 twice daily, and body temperature determined once daily rectally. For infections, animals were
399 anesthetized with isoflurane [rec A/CA/07/2009 (H1N1) (CA09)] or ketamine/xylazine (recRSV-
400 mKate and MA-SARS-CoV-2), followed by intranasal inoculation with 2.5×10^{2}- 2×10^{4} $TCID_{50}$
401 units/animal of GFP-expressing reporter virus version of A/CA/07/2009 (H1N1) (CA09),
402 5.5×10^{5} of recRSV-mKate, or 4.2×10^{5} of MA-SARS-CoV-2. In all cases, virus inoculum was

403 diluted in 50 µl and administered in amounts of 25 µl per nare, followed by treatment with 4'-
404 FlU at specified dose levels and starting time points through oral gavage. Each individual study
405 contained animals receiving equal volumes of vehicle through oral gavage. Animals were
406 euthanized and organs harvested at predefined time points or when animals reached humane
407 study endpoints. At study end point, lung tissue was harvested for virus titration or
408 histopathology.
409

410 **Histopathologic analysis**

411 Lungs were perfused using 10% neutral-buffered formalin, dissected, and fixed. Formalin-fixed
412 lungs were transferred to 70% EtOH, embedded in paraffin, sectioned, stained, and scored by a
413 board-certified veterinary pathologist (KS), who was blinded to the study groups. For each
414 parameter, the most severe lesion in the section was scored. Pleuritis, bronchiolitis, and alveolitis
415 scoring was based on distribution: 1 = focal, 2 = multifocal, 3 = multifocal to coalescing, 4 =
416 diffuse. For interstitial pneumonia (IP): 1 = alveolar septa expanded by 1 leukocyte thickness, 2
417 = 2-leukocytes thick, 3 = 3-leukocytes thick, 4 = 4-leukocytes thick. For vasculitis: 1 = vessel
418 wall infiltrated by leukocytes, 2 = infiltration and separation of myocytes, 3 = same changes as in
419 2 with fibrinoid change. For perivascular cuffing (PVC): 1 = vessels surrounded by 1 leukocyte
420 layer, 2 = 2 to 5-leukocytes thick, 3 = 6 to 10-leukocytes thick, 4 = more than 10-leukocytes
421 thick.

422 **Virus titration**
423

424 Virus samples were serially diluted (10-fold starting at 1:10 initial dilution) in serum-free
425 DMEM (recRSV-mKate and MA-SARS-CoV-2) and supplemented with 0.5% Trypsin (Gibco,
426 recA/California/07/2009). Serial dilutions were added to cells seeded in 96-well plate at

427 1×10^4 cells per well, 24 hours before infection. Infected plates were incubated for 72 hours at
428 37°C with 5% CO_2, and scoring of wells based on reporter activity/syncytia.
429
430 **Virus titration from tissue samples**
431 Organs were weighed and homogenized in 300 µl PBS using a bead beatter, set to 3 cycles of 30
432 seconds each at 4°C, separated by 30-second rest periods. Homogenates were cleared (10
433 minutes at 20,000 × g and 4°C), and cleared supernatants were stored at -80°C until virus
434 titration. Viral titers were expressed as $TCID_{50}$ units per gram input tissue.
435
436 **Neutralization of IL-17 and IL-22**
437 IL-17 (100 µg) and IL-22-Fc (150 µg) neutralizing monoclonal antibody were administered
438 intraperitoneally shortly before microbiota transplantation and virus inoculation thereafter every
439 other day until mice were euthanized.
440
441 **Lung digestion and flow cytometry analysis/isolation of innate immune cells**
442 Lungs were dissected from mice and finely minced with scissors before digestion (40 minutes, at
443 37ºC) with warm RPMI containing 10% FBS, DNase, and 1mg/mL Collagenase type IV
444 (Sigma); lungs were further homogenized via swishing with a 3-mL syringe every 10 minutes
445 during digestion. Following digestion, immune cells were purified with 40%/80% isotonic Percol
446 gradient centrifugation. For flow cytometry analysis, the prepared cells were blocked with 1
447 µg/million cells with 2.4G2 (anti-CD16/anti-CD32) in 100 µL PBS for 15 minutes at 4ºC,
448 followed by 2-times wash with PBS to remove residue of 2.4G2 and then incubated in
449 conjugated mAbs CD45 BV605, MHCII BV650, CD11b APC-Cy7, CD11c BV786, Ly6C

PerCp-Cy5.5, Ly6G AF700, CD64 BV421, CD24 FITC, CD117 GV510, SiglecF PE-CF594, Fcer1 APC. Intracellular staining for cleaved caspase-3 was done using FoxP3 staining buffer purchased from eBioscience. Multi-parameter analysis was performed on a CytoFlex (Beckman Coulter) and analyzed with FlowJo software (Tree Star). Cell sorting was done using Sony SH800Z cell sorter (Sony). Gating strategy for innate immune cells was based on Yu *et al*., [40] and gating strategy for airway epithelial cells was based on Cardani *et al*., [24]. Immune cells and lung airway epithelial subtypes are defined as follow:

Cell Types	**Markers**
Alveolar macrophages	$CD45^+Ly6G^-CD11c^+CD11b^+MHCII^+CD64^+CD24^-Ly6C^+SiglecF^+$
Alveolar macrophages (for cell sorting)	$CD45^+CD11c^+SiglecF^+$
Interstitial macrophages	$CD45^+Ly6G^-CD11c^+CD11b^+MHCII^+CD64^+CD24^-Ly6C^-SiglecF^-$
Exudate macrophages	$CD45^+Ly6G^-CD11c^+CD11b^+MHCII^+CD64^+CD24^-Ly6C^+SiglecF^-$
$CD103^+CD11b^-$ DCs (cDc1)	$CD45^+Ly6G^-CD11c^+CD11b^+MHCII^+CD64^-CD24^+CD11b^-CD103^+$
$CD103^-CD11b^+$ DCs (cDc2)	$CD45^+Ly6G^-CD11c^+CD11b^+MHCII^+CD64^-CD24^+CD11b^+CD103^-$
Neutrophils	$CD45^+Ly6G^+$
Eosinophils	$CD45^+Ly6G^-CD11c^+CD11b^+MHCII^-SiglecF^+$
Basophils	$CD45^+Ly6G^-CD11c^-CD11b^+FceRI^+CD117^-$
Mast cells	$CD45^+Ly6G^-CD11c^-CD11b^+FceRI^+CD117^-$
NK cells	$CD45^+Ly6G^-CD11c^-CD11b^+FceRI^-$
Inflammatory monocytes	$CD45^+Ly6G^-CD11c^+CD11b^+MHCII^-CD64^-Ly6C^+$
Resident monocytes	$CD45^+Ly6G^-CD11c^+CD11b^+MHCII^-CD64^-Ly6C^-$
T cells	$CD45^+Ly6G^-CD11c^-CD11b^-MHCII^-CD24^-FceRI^-$

B cells	$CD45^{+}Ly6G^{-}CD11c^{-}CD11b^{-}MHCII^{+}CD24^{+}FceRI^{-}$
Type 1 airway epithelial cells	$CD45^{-}CD31^{-}EpCAM^{+}T1a^{+}$
Type 2 airway epithelial cells	$CD45^{-}CD31^{-}EpCAM^{+}T1a^{-}MHCII^{+}$
Conducting airway epithelial cells	$CD45^{-}CD31^{-}EpCAM^{+}T1a^{-}MHCII^{-}$

457

458 **RNA-Seq**

459 RNA was isolated from lungs or FACs-sorted alveolar macrophages using RNeasy Plus Mini Kit
460 from Qiagen. The prepared RNA samples were then sent to the Molecular Evolution Core of
461 Georgia Institute of Technology for library preparation and sequencing on the NextSeq
462 instrument with a high output 2x75bp run. FASTQC was used for sequencing reads quality
463 screening. The RNAseq data were then analyzed using the Galaxy server.

464

465 **Adoptive transfer of alveolar macrophages**

466 Lungs were harvested from CD45.1 mice and digested with Collagenase type IV as described
467 above. Alveolar macrophages (defined at $CD45^{+}MHCII^{+}CD11c^{+}Siglect^{+}$) were stained and
468 FACs-sorted. Small aliquot of isolated cells was used to determined purity. Unless stated
469 otherwise, $5x10^{5}$ alveolar macrophages in 30 µl PBS were administered intranasally to recipient
470 mice. One day post cells transfer, some mice were euthanized to determine transfer efficiency
471 and survival of transferred cells; and some mice were inoculated with IAV. For survival
472 experiments, mice were monitored twice daily for 14 days. For lung virus titers, mice were
473 euthanized on day 4.5 post virus inoculation.

474

475 **Ex vivo inhibiting Notch4 signaling in alveolar macrophages.**

476 Alveolar macrophages were FACS-sorted as described. After sorting, cells were treated with
477 either isotype control antibody (Cat# BE0091, BioXCell) or an anti-Notch4 monoclonal antibody
478 (20µg/mL) (Cat# BE0129, BioXCell), known to neutralize Notch 4 [27] for 30 minutes. Cells
479 were washed twice and resuspended in PBS and intranasally transferred to mice.
480
481 ***Ex vivo* alveolar macrophages culture, virucidal assay, and anti-body mediated removal of**
482 **C1qa.** Alveolar macrophages were FACS-sorted as described. After sorted cells were incubated
483 for 18h at 37ºC. Cells were washed twice with serum-free media and were incubated with live
484 CA09 (MOI = 1) in serum-free DMEM supplemented with 0.5% Trypsin (flu media) for 45min.
485 In addition, to assess whether alveolar macrophages are the terminal destination for IAV, some
486 cells had new flu media added and were incubated for another 24h. Viral titer and genomes were
487 determined via $TCID_{50}$ and PCR methods. **Antibody-mediated removal of C1qa from ex vivo**
488 **alveolar macrophages' supernatants.** Cell-free supernatants of 18h AM cultures were treated
489 with C1qa polyclonal antibodies or isotype for 2 hours at 4ºC and protein A/G was added and
490 centrifuged. Supernatant was harvested and incubated with CA09 stocks for 45mins, at which
491 point IAV infection titers were assayed.
492
493 **Ex Vivo alveolar AM bead uptake (i.e.** Phagocytosis) assay was performed with Phagocytosis
494 assay kit (Cat#500290, Cayman chemical). Alveolar macrophages were FACs-sorted as
495 described. After sorting, $1x10^5$ cells were seeded in each well of a 96-well plate and incubated
496 for 18 h at 37ºC. Cells were washed twice, and IgG-FITC beads were added and incubated for 2
497 hours at 37ºC. After incubation period, cells were centrifuged, and supernatants were removed

498 and resuspended 300µl of FACs buffer. Level of cell fluorescence, an indicator of bead uptake,
499 was measured via flow cytometry.
500
501 **Quantitative real-time PCR**
502 Total RNA from lungs or from FACs-sorted alveolar macrophages were isolated using the
503 Qiagen RNeasy Mini Kit with on-column DNase digestion according to manufacturer's protocol.
504 cDNA was generated using the Superscript First Strand Synthesis kit for RT-PCR and random
505 hexamer primers (Invitrogen). Q-PCR was performed with SYBR Green using StepOnePlus
506 PCR system (Applied Biosystem), and all genes expression was normalized to GAPDH. Primer
507 sequences are shown in Table 1.
508
509 **Quantification and statistical analysis**
510 Results were expressed as mean ± SEM. All data was plotted in GraphPad Prism version 10.
511 Statistical significance was assessed by One-way ANOVA, Student's t test, and Two-way
512 ANOVA. Differences between experimental groups were considered significant if *$p<0.05$,
513 **$p<0.01$, ***$p<0.001$, ****$p<0.0001$.
514

Table 1 qPCR primers		
Genes	**Forward 5' --> 3'**	**Reverse 5' --> 3'**
Notch4	GAACGCGACATCAACGAGTG	GGAACCCAAGGTGTTATGGCA
Retlna	CCAATCCAGCTAACTATCCCTCC	ACCCAGTAGCAGTCATCCCA
CD209g	GGCCTCAGCGATCACAGAAG	ACAACGGCTGTCATTCCATTTA
Abca9	TCGATAGATGCAGTGAGAGTCA	CACAAGGAGCTGAATGGTCTTT
Tsc22d3	CTGTTGGCCTCGACTGCTG	GCCGAAAGTTGCTCACGAAG
Sik1	TCATGTCGGAGTTCAGTGCG	ACCTGCGTTTTGGTGACTCG
Fcrls	CTTCTGGTCTTCGCTCCTGTC	ATGGTGTAGCTTGAAGCACTG
Dmkn	AGCTGACCAGTTTTCTAAGCC	GCCAGTTGTAAGTAGGATTCACC
F13a1	GAGCAGTCCCGCCCAATAAC	CCCTCTGCGGACAATCAACTTA
Ccl24	TCTTGCTGCACGTCCTTTATT	GCATCCAGTTTTTGTATGTGCC
Ifitm1	GACAGCCACCACAATCAACAT	CCCAGGCAGCAGAAGTTCAT
Ltb4r1	ATGGCTGCAAACACTACATCTC	GACCGTGCGTTTCTGCATC
Akr1b8	GACCAAGGCAGAATCCTCACC	AGATGCCCTTCGAGTGACAGT
C1qa	AAAGGCAATCCAGGCAATATCA	TGGTTCTGGTATGGACTCTCC
Maf	AGGAGGAGGTCATCCGACTG	CTTCTCGCTCTCCAGAATGTG
Procr	AATGCCTACAACCGGACTCG	ACCAGTGATGTGTAAGAGCGA
Socs3	ATGGTCACCCACAGCAAGTTT	TCCAGTAGAATCCGCTCTCCT
Marcksl1	CAATGGAGACTTAACCCCCAAG	GGCCACTCAATTTGAAAGGCT
Kcnn4	GCTCAACCAAGTCCGCTTC	GTGATCGGAATCAGCCACAGT
Tmem119	CCTACTCTGTGTCACTCCCG	CACGTACTGCCGGAAGAAATC
Acpp	CATTGGTGTTTCGGCATGGAG	CCAAGTTCGTAGTGCTGTTCC
Gucy2c	GACTTTTCTCTCGCTTACTTGGA	TGAATGCACGAGCAAACTTGG
Il6	TGGGGCTCTTCAAAAGCTCC	AGGAACTATCACCGGATCTTCAA
Ifnb1	CAGCTCCAAGAAAGGACGAAC	GGCAGTGTAACTCTTCTGCAT
Cxcl10	CCAAGTGCTGCCGTCATTTTC	GGCTCGCAGGGATGATTTCAA
Cxcl11	GGCTTCCTTATGTTCAAACAGGG	GCCGTTACTCGGGTAAATTACA
Irf7	GAGACTGGCTATTGGGGGAG	GACCGAAATGCTTCCAGGG
Isg15	GGTGTCCGTGACTAACTCCAT	TGGAAAGGGTAAGACCGTCCT
Oas3	TCTGGGGTCGCTAAACATCAC	GATGACGAGTTCGACATCGGT
Oasl1	CAGGAGCTGTACGGCTTCC	CCTACCTTGAGTACCTTGAGCAC
Oasl2	TTGTGCGGAGGATCAGGTACT	TGATGGTGTCGCAGTCTTTGA
Ifit1	CTGAGATGTCACTTCACATGGAA	GTGCATCCCCAATGGGTTCT
Ifit2	AGTACAACGAGTAAGGAGTCACT	AGGCCAGTATGTTGCACATGG
Ifit3	CTGAAGGGGAGCGATTGATT	AACGGCACATGACCAAAGAGTAGA
Gapdh	TGGATTTGGACGCATTGGTC	TTTGCACTGGTACGTGTTGAT
Inf-NA	CAATTCAACTTGGGAATCAAAATCAGA	CTGACTGTCCAGCAGCAAAGTT
Inf-M	TGTAAAACGACGGCCAGTAGCAAAAGCAGGTAG	CAGGAAACAGCTATGACCAGTAGMAACAAGGTAG
	AGAAAAGAATGTAACAGTAACACACTCTGT	TGTTTCCACAATGTARGACCAT

Influenza A H1N1pdm09 HA genes	Probes 5'-(FAM)-CAGCCAGCAATRTTRCATTTACC-(MGB)-3'

515

516

Table S2. FACs antibodies					
Specificity	**Clone**	**Fluorochrome**	**Supplier**	**Catalog#**	**Dilution**
CD45	30-F11	BV605	Biolegend	103155	1/800
Ly6G	1A8	AF700	BD Biosciences	561236	1/200
Ly6C	HK1.4	PercP-Cy5.5	Thermo Fisher	45-5932	1/200
CD11b	M1/70	APC-Cy7	BD Biosciences	557657	1/200
CD11c	HL3	BV786	BD Biosciences	563786	1/100
MHCII	M5/114.15.2	BV650	BD Biosciences	563415	1/1000
CD64	X54-5/7.1	BV421	Biolegend	139309	1/400
CD24	M1/69	FITC	BD Biosciences	553261	1/1000
CD117	ACK2	BV510	Biolegend	135119	1/100
SiglecF	E50-2440	PE-CF594	BD Biosciences	562757	1/1000
Fcer1	Mar-1	APC	Thermo Fisher	175898-80	1/100
Capse-3	269518	APC	R&D System	IC835R-100UG	1/50
CD86	GL-1	APC	Biolegend	105012	1/100
CD206	C068C2	APC-AF700	Biolegend	141708	1/100
CD200R	OX-90	PE	BD Biosciences	565543	1/100
CD45.1	A20	PE-Cy7	Thermo Fisher	25-0453-82	1/100
CD45.2	104	FITC	BD Biosciences	561874	1/100
T1a (Podoplanin)	8.1.1	PE	Biolegend	127408	1/100
CD31	MEC13.3	APC	Biolegend	102510	1/100
EpCam	G8.8	AF700	BioLegend	118240	1/100

517

Acknowledgments:

We thank Tim Denning and Ifor Williams for insightful guidance. We thank RS Baric for SARS-CoV-2 MA10 virus isolate and Georgia State University's High Containment Core and Division of Animal Resources for support. **Funding**: This work was supported, in part, by Public Health Service grants AI141222 (to RKP), AI171403 (to RKP), and AI170014 (to ATG) from the NIH/NIAID. The funders had no role in study design, data collection and interpretation, or the decision to submit the work for publication. **Author contributions:** Conceptualization: RKP, ATG. Investigation: VLN, CML, KS. Resources: RKP, ATG. Visualization: VLN, CML, KS, RKP, ATG. Validation: RKP, ATG. Funding acquisition: RKP. Project administration: RKP, ATG. Supervision: RKP, ATG, MK. Writing – original draft: ATG. Writing – review & editing: VLN, CML, KS, RKP. **Competing interests:** RKP reports contract testing from Enanta Pharmaceuticals and Atea Pharmaceuticals, and research support from Gilead Sciences, outside of the described work. All other authors declare that they have no competing interests. **Data and materials availability:** All data are available in the main text or the supplementary materials. Materials and methods are available as supplementary materials at the Science website.

535

536 **References**

537 [1] V.L. Ngo, A.T. Gewirtz, Microbiota as a potentially-modifiable factor influencing COVID-
538 19, Curr Opin Virol, 49 (2021) 21-26.
539 [2] P. Brodin, Immune-microbe interactions early in life: A determinant of health and disease
540 long term, Science, 376 (2022) 945-950.
541 [3] L.K. Beura, S.E. Hamilton, K. Bi, J.M. Schenkel, O.A. Odumade, K.A. Casey, E.A.
542 Thompson, K.A. Fraser, P.C. Rosato, A. Filali-Mouhim, R.P. Sekaly, M.K. Jenkins, V. Vezys,
543 W.N. Haining, S.C. Jameson, D. Masopust, Normalizing the environment recapitulates adult
544 human immune traits in laboratory mice, Nature, 532 (2016) 512-516.
545 [4] S.P. Rosshart, B.G. Vassallo, D. Angeletti, D.S. Hutchinson, A.P. Morgan, K. Takeda, H.D.
546 Hickman, J.A. McCulloch, J.H. Badger, N.J. Ajami, G. Trinchieri, F. Pardo-Manuel de Villena,
547 J.W. Yewdell, B. Rehermann, Wild Mouse Gut Microbiota Promotes Host Fitness and Improves
548 Disease Resistance, Cell, 171 (2017) 1015-1028 e1013.
549 [5] J. Phelan, Choosing a Health Standard for Your Model, 2016.
550 https://www.taconic.com/taconic-insights/quality/choosing-rodent-model-health-standards.html
551 [6] M.J. Korth, N. Tchitchek, A.G. Benecke, M.G. Katze, Systems approaches to influenza-virus
552 host interactions and the pathogenesis of highly virulent and pandemic viruses, Semin Immunol,
553 25 (2013) 228-239.
554 [7] Ivanov, II, D.R. Littman, Segmented filamentous bacteria take the stage, Mucosal Immunol,
555 3 (2010) 209-212.

556 [8] F. Teng, C.N. Klinger, K.M. Felix, C.P. Bradley, E. Wu, N.L. Tran, Y. Umesaki, H.J. Wu,
557 Gut Microbiota Drive Autoimmune Arthritis by Promoting Differentiation and Migration of
558 Peyer's Patch T Follicular Helper Cells, Immunity, 44 (2016) 875-888.
559 [9] Z. Shi, J. Zou, Z. Zhang, X. Zhao, J. Noriega, B. Zhang, C. Zhao, H. Ingle, K. Bittinger, L.M.
560 Mattei, A.J. Pruijssers, R.K. Plemper, T.J. Nice, M.T. Baldridge, T.S. Dermody, B. Chassaing,
561 A.T. Gewirtz, Segmented Filamentous Bacteria Prevent and Cure Rotavirus Infection, Cell, 179
562 (2019) 644-658 e613.
563 [10] M. Zemlin, M. Hummel, I. Anagnostopoulos, H. Stein, Improved polymerase chain reaction
564 detection of clonally rearranged T-cell receptor beta chain genes, Diagn Mol Pathol, 7 (1998)
565 138-145.
566 [11] M. Wymore Brand, M.J. Wannemuehler, G.J. Phillips, A. Proctor, A.M. Overstreet, A.E.
567 Jergens, R.P. Orcutt, J.G. Fox, The Altered Schaedler Flora: Continued Applications of a
568 Defined Murine Microbial Community, ILAR J, 56 (2015) 169-178.
569 [12] A.H. Newton, A. Cardani, T.J. Braciale, The host immune response in respiratory virus
570 infection: balancing virus clearance and immunopathology, Semin Immunopathol, 38 (2016)
571 471-482.
572 [13] C. Purnama, S.L. Ng, P. Tetlak, Y.A. Setiagani, M. Kandasamy, S. Baalasubramanian, K.
573 Karjalainen, C. Ruedl, Transient ablation of alveolar macrophages leads to massive pathology of
574 influenza infection without affecting cellular adaptive immunity, Eur J Immunol, 44 (2014)
575 2003-2012.
576 [14] C.M. Lieber, M. Aggarwal, J.J. Yoon, R.M. Cox, H.J. Kang, J. Sourimant, M. Toots, S.K.
577 Johnson, C.A. Jones, Z.M. Sticher, A.A. Kolykhalov, M.T. Saindane, S.M. Tompkins, O. Planz,
578 G.R. Painter, M.G. Natchus, K. Sakamoto, R.K. Plemper, 4'-Fluorouridine mitigates lethal

579 infection with pandemic human and highly pathogenic avian influenza viruses, PLoS Pathog, 19
580 (2023) e1011342.
581 [15] J. Sourimant, C.M. Lieber, M. Aggarwal, R.M. Cox, J.D. Wolf, J.J. Yoon, M. Toots, C. Ye,
582 Z. Sticher, A.A. Kolykhalov, L. Martinez-Sobrido, G.R. Bluemling, M.G. Natchus, G.R. Painter,
583 R.K. Plemper, 4'-Fluorouridine is an oral antiviral that blocks respiratory syncytial virus and
584 SARS-CoV-2 replication, Science, 375 (2022) 161-167.
585 [16] C. Schneider, S.P. Nobs, A.K. Heer, M. Kurrer, G. Klinke, N. van Rooijen, J. Vogel, M.
586 Kopf, Alveolar macrophages are essential for protection from respiratory failure and associated
587 morbidity following influenza virus infection, PLoS Pathog, 10 (2014) e1004053.
588 [17] G. Dranoff, A.D. Crawford, M. Sadelain, B. Ream, A. Rashid, R.T. Bronson, G.R.
589 Dickersin, C.J. Bachurski, E.L. Mark, J.A. Whitsett, et al., Involvement of granulocyte-
590 macrophage colony-stimulating factor in pulmonary homeostasis, Science, 264 (1994) 713-716.
591 [18] T. Thepen, N. Van Rooijen, G. Kraal, Alveolar macrophage elimination in vivo is
592 associated with an increase in pulmonary immune response in mice, J Exp Med, 170 (1989) 499-
593 509.
594 [19] R. Rauschmeier, C. Gustafsson, A. Reinhardt, A.G. N, L. Tortola, D. Cansever, S.
595 Subramanian, R. Taneja, M.J. Rossner, M.H. Sieweke, M. Greter, R. Mansson, M. Busslinger, T.
596 Kreslavsky, Bhlhe40 and Bhlhe41 transcription factors regulate alveolar macrophage self-
597 renewal and identity, EMBO J, 38 (2019) e101233.
598 [20] S.M. Behar, C.J. Martin, M.G. Booty, T. Nishimura, X. Zhao, H.X. Gan, M. Divangahi,
599 H.G. Remold, Apoptosis is an innate defense function of macrophages against Mycobacterium
600 tuberculosis, Mucosal Immunol, 4 (2011) 279-287.

601 [21] S.J. Allden, P.P. Ogger, P. Ghai, P. McErlean, R. Hewitt, R. Toshner, S.A. Walker, P.
602 Saunders, S. Kingston, P.L. Molyneaux, T.M. Maher, C.M. Lloyd, A.J. Byrne, The Transferrin
603 Receptor CD71 Delineates Functionally Distinct Airway Macrophage Subsets during Idiopathic
604 Pulmonary Fibrosis, Am J Respir Crit Care Med, 200 (2019) 209-219.
605 [22] M.P. Kuczma, E.A. Szurek, A. Cebula, B. Chassaing, Y.J. Jung, S.M. Kang, J.G. Fox, B.
606 Stecher, L. Ignatowicz, Commensal epitopes drive differentiation of colonic T(regs), Sci Adv, 6
607 (2020) eaaz3186.
608 [23] T. Ruan, J. Sun, W. Liu, R.A. Prinz, D. Peng, X. Liu, X. Xu, H1N1 Influenza Virus Cross-
609 Activates Gli1 to Disrupt the Intercellular Junctions of Alveolar Epithelial Cells, Cell Rep, 31
610 (2020) 107801.
611 [24] A. Cardani, A. Boulton, T.S. Kim, T.J. Braciale, Alveolar Macrophages Prevent Lethal
612 Influenza Pneumonia By Inhibiting Infection Of Type-1 Alveolar Epithelial Cells, PLoS Pathog,
613 13 (2017) e1006140.
614 [25] A.V. Misharin, L. Morales-Nebreda, G.M. Mutlu, G.R. Budinger, H. Perlman, Flow
615 cytometric analysis of macrophages and dendritic cell subsets in the mouse lung, Am J Respir
616 Cell Mol Biol, 49 (2013) 503-510.
617 [26] D. Berrebi, S. Bruscoli, N. Cohen, A. Foussat, G. Migliorati, L. Bouchet-Delbos, M.C.
618 Maillot, A. Portier, J. Couderc, P. Galanaud, M. Peuchmaur, C. Riccardi, D. Emilie, Synthesis of
619 glucocorticoid-induced leucine zipper (GILZ) by macrophages: an anti-inflammatory and
620 immunosuppressive mechanism shared by glucocorticoids and IL-10, Blood, 101 (2003) 729-
621 738.

622 [27] M. Xia, H. Harb, A. Saffari, C. Sioutas, T.A. Chatila, A Jagged 1-Notch 4 molecular switch
623 mediates airway inflammation induced by ultrafine particles, J Allergy Clin Immunol, 142
624 (2018) 1243-1256 e1217.
625 [28] P.M. Varghese, U. Kishore, R. Rajkumari, Human C1q Regulates Influenza A Virus
626 Infection and Inflammatory Response via Its Globular Domain, Int J Mol Sci, 23 (2022).
627 [29] L.B. Klickstein, S.F. Barbashov, T. Liu, R.M. Jack, A. Nicholson-Weller, Complement
628 receptor type 1 (CR1, CD35) is a receptor for C1q, Immunity, 7 (1997) 345-355.
629 [30] M.C. Abt, L.C. Osborne, L.A. Monticelli, T.A. Doering, T. Alenghat, G.F. Sonnenberg,
630 M.A. Paley, M. Antenus, K.L. Williams, J. Erikson, E.J. Wherry, D. Artis, Commensal bacteria
631 calibrate the activation threshold of innate antiviral immunity, Immunity, 37 (2012) 158-170.
632 [31] T. Ichinohe, I.K. Pang, Y. Kumamoto, D.R. Peaper, J.H. Ho, T.S. Murray, A. Iwasaki,
633 Microbiota regulates immune defense against respiratory tract influenza A virus infection, Proc
634 Natl Acad Sci U S A, 108 (2011) 5354-5359.
635 [32] H. Chen, L. Wang, X. Wang, X. Wang, H. Liu, Y. Yin, Distribution and Strain Diversity of
636 Immunoregulating Segmented Filamentous Bacteria in Human Intestinal Lavage Samples,
637 Microb Ecol, 79 (2020) 1021-1033.
638 [33] H. Jonsson, L.W. Hugerth, J. Sundh, E. Lundin, A.F. Andersson, Genome sequence of
639 segmented filamentous bacteria present in the human intestine, Commun Biol, 3 (2020) 485.
640 [34] S. Subramanian, C.J. Busch, K. Molawi, L. Geirsdottir, J. Maurizio, S. Vargas Aguilar, H.
641 Belahbib, G. Gimenez, R.A.A. Yuda, M. Burkon, J. Favret, S. Gholamhosseinian Najjar, B. de
642 Laval, P.K. Kandalla, S. Sarrazin, L. Alexopoulou, M.H. Sieweke, Long-term culture-expanded
643 alveolar macrophages restore their full epigenetic identity after transfer in vivo, Nat Immunol, 23
644 (2022) 458-468.

645 [35] T. Wang, J. Zhang, Y. Wang, Y. Li, L. Wang, Y. Yu, Y. Yao, Influenza-trained mucosal-
646 resident alveolar macrophages confer long-term antitumor immunity in the lungs, Nat Immunol,
647 24 (2023) 423-438.
648 [36] A.K. Verma, S. Bansal, C. Bauer, A. Muralidharan, K. Sun, Influenza Infection Induces
649 Alveolar Macrophage Dysfunction and Thereby Enables Noninvasive Streptococcus pneumoniae
650 to Cause Deadly Pneumonia, J Immunol, 205 (2020) 1601-1607.
651 [37] A. Nogales, G. Avila-Perez, J. Rangel-Moreno, K. Chiem, M.L. DeDiego, L. Martinez-
652 Sobrido, A Novel Fluorescent and Bioluminescent Bireporter Influenza A Virus To Evaluate
653 Viral Infections, J Virol, 93 (2019).
654 [38] A.L. Hotard, F.Y. Shaikh, S. Lee, D. Yan, M.N. Teng, R.K. Plemper, J.E. Crowe, Jr., M.L.
655 Moore, A stabilized respiratory syncytial virus reverse genetics system amenable to
656 recombination-mediated mutagenesis, Virology, 434 (2012) 129-136.
657 [39] K.H. Dinnon, 3rd, S.R. Leist, A. Schafer, C.E. Edwards, D.R. Martinez, S.A. Montgomery,
658 A. West, B.L. Yount, Jr., Y.J. Hou, L.E. Adams, K.L. Gully, A.J. Brown, E. Huang, M.D.
659 Bryant, I.C. Choong, J.S. Glenn, L.E. Gralinski, T.P. Sheahan, R.S. Baric, A mouse-adapted
660 model of SARS-CoV-2 to test COVID-19 countermeasures, Nature, 586 (2020) 560-566.
661 [40] Y.R. Yu, E.G. O'Koren, D.F. Hotten, M.J. Kan, D. Kopin, E.R. Nelson, L. Que, M.D. Gunn,
662 A Protocol for the Comprehensive Flow Cytometric Analysis of Immune Cells in Normal and
663 Inflamed Murine Non-Lymphoid Tissues, PLoS One, 11 (2016) e0150606.

664

665

666 **FIGURE LEGENDS**

667 **Figure 1. Colonization of the intestine with SFB protected mice from influenza virus**
668 **infection.**

669 **(A)** EF and SPF mice were inoculated with A/CA/07/2009 (H1N1) influenza virus (CA09) as
670 schematized. Lung viral titers, survival, body weight, and temperature were monitored.

671 **(B)** As schematized, conventionally colonized SFB^- mice received feces that lacked SFB (SFB^-),
672 contained SFB (SFB^+), or contained SFB but no other bacteria (SFB-MA). Seven days after post-
673 transplant, mice were inoculated with CA09. Mice were euthanized 4.5-days later or monitored
674 daily for survival, body weight, and temperature for 2 weeks.

675 **(C)** SFB^- mice were administered SFB 3 months or 7 days prior to CA09 inoculation. **(i)** qRT-
676 PCR analysis of SFB colonization level over the course of 14 weeks. **(ii)** Mice were euthanized
677 4.5-days later or monitored daily for survival, body weight, and temperature for 2 weeks.

678 **(D)** qRT-PCR analysis of SFB level in the small intestine, lungs, and spleens after 7 days
679 colonization.

680 **(E)** SFB^- mice were untreated (naïve) or administrated SFB. Seven days later, mice were
681 inoculated (or not) with CA09. Mice were euthanized 4.5 days later. H&E staining lung sections
682 scored for pleuritis, bronchiolitis, alveolitis, vasculitis, interstitial pneumonia (IP), and
683 perivascular cuffing (PVC).

684 All experiments n = 5 mice per group. Data is representative of two to three independent
685 experiments. yielding an identical pattern of results. Statistical analysis; Viral titer: One-way
686 ANOVA or student *t* test. survival: Log-rank Mantel-Cox test. Body weights and temperature:
687 Two-way ANOVA. *$p<0.05$, **$p<0.01$, ***$p<0.001$, ns not significant.

688

689 **Figure 2. SFB mediated protection against IAV was maintained in an array of knockout**

690 **mice and did not require complex gut microbiota.**

691 Lung viral titer, survival rate, body weight change, and temperature of: SFB-negative mice were

692 colonized with SFB for 7 days then inoculated with CA09.

693 **(A)** *rag1*$^{-/-}$ mice

694 **(B)** mice received neutralization of IL-17/IL-22 monoclonal antibodies every other day

695 throughout the experiment

696 **(C)** *Ifnar*$^{-/-}$ mice

697 **(D)** *rag1*$^{-/-}$*yc*$^{-/-}$ mice

698 **(E)** *stat1*$^{-/-}$ mice

699 **(F)** Altered Schaedler flora (ASF) mice.

700 All experiments n = 5 mice per group. Statistical analysis; Viral titer: student *t* test, Survival:

701 Log-rank Mantel-Cox test. Body weights and temperature: Two-way ANOVA. **$p<0.01$,

702 ***$p<0.001$.

703

704 **Figure 3. SFB's protection against IAV infection associated with preservation of resident**
705 **lung phagocytes.**
706 **(A)** SFB^{-} mice were untreated (naïve) or administrated SFB. Seven days later, mice were
707 inoculated (or not) with CA09. Mice were euthanized 4.5-days later. **(i)** Whole lung gene
708 expression assayed by RNA-seq and data are heatmap of genes that are significantly altered by
709 2-fold in all treatment groups relative to the naïve group. **(ii)** Quantitation of CA09 level in these
710 extracts by qRT-PCR.
711 **(B)** SFB^{-} mice were untreated (naïve) or administrated SFB. Seven days later, mice were
712 inoculated (or not) with CA09. Mice were euthanized 4.5-days later, and lung assayed by flow
713 cytometry. **(i & ii)** Analysis of dendritic cells and alveolar macrophage; representative flow plot
714 and frequencies and cell numbers **(i)** cDC1. **(ii)** alveolar macrophages. **(iii)** Frequencies and cell
715 numbers of lung neutrophils, inflammatory monocytes, and NK cells.
716 **(C) (i)** Experimental schema: SFB^{-} mice colonized with SFB, inoculated with CA09, and treated
717 with 4'-FlU at indicated doses. On day 4.5 post virus inoculation, mice were euthanized, and
718 lungs were harvested to determine virus titers and FACs analysis. **(ii)** lung viral titer. **(iii)** FACs
719 plot graphical representation, frequencies, and cell numbers of lung cDC1, and AMs. **(iv)** Cell
720 numbers of lung neutrophils, inflammatory monocytes, and NK cells.
721 All experiment n = 4-5 per group. Data is representative of two to three independent experiments
722 (B and C), yielding an identical pattern of results. Statistical analysis: One-way ANOVA.
723 *$p<0.05$, **$p<0.01$, ***$p<0.001$, ****$p<0.0001$, ns not significant.
724

725 **Figure 4. SFB-mediated protection against IAV infection and resulting disease required**
726 **alveolar macrophages.**
727 **(A-B) (A)** *batf3*$^{-/-}$ and **(B)** *csf2*$^{-/-}$ mice were administered SFB and then, 7 days later, inoculated
728 with CA09. Lung viral titer, body weight change, temperature, and survival were monitored.
729 **(C) (i-ii)** SFB^{-} mice were orally administered with clodronate liposomes one day before mice
730 were euthanized. FACS analysis to determine the AMs depletion efficacy after clodronate
731 treatment. **(i)** FACS graphical representation of lung AMs, frequency of lung AMs and others
732 immune cells after clodronate treatment. **(ii)** SFB^{-} mice were colonized with SFB for 7 days, and
733 clodronate liposomes were orally administered to mice one day before CA09 inoculation. Mice
734 were euthanized on day 4 post-virus inoculation. Lung viral titer, survival rate, body weight,
735 temperature was measured.
736 **(D)** SFB^{-} mice were untreated (naïve) or administrated SFB. Seven days later, mice were
737 inoculated (or not) with CA09. Mice were euthanized 4.5-days later. Level of cleaved caspase-3
738 of alveolar macrophages in lung were measured with FACS
739 **(E)** SFB^{-} mice were untreated or treated as in (D). Level of CD71 expression of alveolar
740 macrophages in lung were measured with FACS.
741 **(F)** SFB^{-} mice treated as described in (C) FACS plot graphical representation, and frequencies
742 CA09 level in T1ACEs, T2AECs, and Conducting AECs were assayed by flow cytometry.
743 All experiment n = 5 mice per group. Data is representative of two to three independent
744 experiments (B-F), yielding an identical pattern of results. Statistical analysis; Viral titer, relative
745 SFB genomes, MFI, frequencies/cell numbers of immune cell data: One-way ANOVA or student
746 *t* test. Survival data Log-rank Mantel-Cox. Body weights, temperature: Two-way ANOVA.
747 *$p<0.05$, ***$p<0.001$, ****$p<0.0001$, ns not significant.

748 **Figure 5. SFB colonization intrinsically altered AM to withstand IAV-induced depletion.**

749 As schematized, SFB^{-} CD45.1 mice were administered with SFB or PBS. Seven days later, AM
750 were isolated by FACs-sorting, and transferred to SFB- CD45.2 mice. One day post-transferred,
751 mice were inoculated with CA09. Four days later, lungs were harvested, and AM analyzed by
752 FACs. Representative FACs plots, cell frequencies, cell numbers, and cleaved caspase-3 level
753 are shown.

754 All experiment n = 5 mice per group. Data is representative of two independent experiments (B-
755 F), yielding an identical pattern of results. Statistical test: One-way ANOVA. **$p<0.01$,
756 ***$p<0.001$, ****$p<0.0001$, ns not significant.

757

758 **Figure 6. SFB$^+$ AM exhibited inflammatory anergy and enhanced antiviral function ex**
759 **vivo.**

760 **(A)** Schematic design for ex vivo studies of AM.

761 **(B)** Comparison of basal SFB$^+$ and SFB$^-$ AM gene expression by RNA-seq, shown as a volcano
762 plot.

763 **(C)** SFB$^+$ and SFB$^-$ AM were exposed to UV-CA09 with or without Notch4 neutralizing, or
764 isotype control antibodies. RNA was harvested 24 hours later, and gene expression assayed by
765 RT-qPCR. Results are a heat map summary with full results shown in FS7.

766 **(D)** AM and CA09 stocks were incubated at 37C, or indicated temperature, for 45 minutes and
767 supernatant were collected. In addition, some cells had new media added and were incubated for
768 another 24 hours. **(i)** virus infection titers in supernatant at 45 minutes and 24 hours were
769 assayed. **(ii)** Supernatant were collected after 45 minutes incubated with CA09 and viral
770 genomes quantitated by RT-qPCR. **(iii)** Cell-free supernatant of 15 hours AM cultures were
771 incubated with live CA09 stocks, with or without C1qa-neutralization or isotype antibody for 45
772 minutes, at which point virus infection titers were assayed. **(iv)** Cell lysates were generated upon
773 CA09 removal or 24 hours later and viral genomes quantitated by RT-qPCR.

774 All experiment n = 4-5 mice per group. Data is representative of two independent experiments,
775 yielding an identical pattern of results. Statistical analysis: One-way ANOVA. *$p<0.05$,
776 **$p<0.01$, , ****$p<0.0001$, ns not significant.

777

Figure 7. Adoptive transfer of SFB$^+$ AM enabled recipients to better manage IAV infection.

(A) As schematized, SFB$^-$ mice were administered SFB or PBS. Seven days later, AMs were isolated by FACs-sorting and transferred to SFB$^-$ mice. Mice were administered 5x10^5 cells per mouse. One day post adoptive transfer, mice were inoculated with a lethal dose of CA09. Mice were euthanized 4.5 days post-inoculation for viral titer and gross lung assessment or monitored for survival, body weight, and temperature.

(B) As schematized, AMs from SFB$^-$ *csf2*$^{+/+}$ mice were administered SFB or PBS. Seven days later, AMs were isolated by FACs-sorting and transferred to SFB$^-$ *csf2*$^{-/-}$ mice. One day post-transfer, mice were inoculated with CA09. Mice were monitored for 14 days for clinical symptoms including survival rate, body weight, and temperature.

(C) SFB$^-$ mice were administered clodronate liposomes to remove endogenous AM populations. Seven days later after initiation of depletion, mice were administered 5x10^5 AM cells harvested from the SFB$^-$ or SFB$^+$ mice. One day post transfer, mice were inoculated with CA09. Mice were euthanized on day four to assess lung viral titer and gross lung assessment or monitored for survival, body weight, and temperature.

All experiments have at least n = 5 mice per group. Data is representative of two independent experiments (A), yielding an identical pattern of results. Statistical analysis; One-way ANOVA: viral titers. Survival: Log-rank Mantel-Cox test. Body weight, temperature: Two-way ANOVA. *$p<0.05$, **$p<0.01$, ****$p<0.0001$, ns not significant.

798 **Figure S1. Feces from SFB-monoassociated mice, but not germfree mice, protected mice**
799 **against IAV infection, Related to Figure 1.**

800 **(A)** As schematized, SFB^- mice were colonized with complex microbiota that does not contain
801 SFB or PBS or germ-free microbiota or gnotobiotic SFB-monoassociated. Seven days post
802 colonization, mice inoculated with CA09, and were monitored for 14 days for clinical signs or
803 were euthanized on day 4.5 post-virus inoculation to determined lung viral titer. Lung viral titer,
804 survival rate, body weight and temperature.

805 **(B)** SFB^- mice were colonized with SFB as indicated time point. After colonization period, mice
806 were inoculated with CA09. Viral titer and clinical signs were assessed as in (B).

807 **(C)** As schematized, 24 weeks old SFB^- mice were colonized with SFB for seven days and then
808 inoculated with CA09. Viral titer and clinical signs were assessed as in (B).

809 All experiments at least n = 5 mice per group. Data is representative of two independent
810 experiments (A and B), yielding an identical pattern of results. Statistical analysis; One-way
811 ANOVA: viral titers. Survival: Log-rank Mantel-Cox test. Body weight, temperature: Two-way
812 ANOVA. *$p<0.05$, **$p<0.01$, ***$p<0.001$, ****$p<0.0001$, ns not significant.

813

814

815 **Figure S2. SFB colonization prevented IAV-induced changes in lung cellularity, Related to**
816 **Figure 3.**

817 **(A)** Gating strategy for identification of immune cells.

818 **(B)** SFB^- mice were colonized with SFB for seven days then inoculated with CA09. On day 4.5
819 post virus inoculation were lung assayed by flow cytometry. Frequencies and cell numbers of
820 indicated immune cells.

821 **(C) (i)** Experimental schema: SFB^- mice were colonized with SFB for seven days before CA09
822 inoculation. Mice were euthanized on one-, two-, and four-day post-virus inoculation. **(ii)** CA09
823 viral genomes quantitated by RT-qPCR. **(iii)** FACs graphical representation, frequency, cell
824 numbers, and cleaved caspase-3 mean fluorescence intensity of lung AMs. **(iv)** Frequencies and
825 cell numbers of lungs' innate immune cells.

826 All experiments n = 5 mice per group. Data is representative of two to three independent
827 experiments (B), yielding an identical pattern of results. Statistical analysis: One-way ANOVA:
828 B, Two-way ANOVA: C. *$p<0.05$, **$p<0.01$, ***$p<0.001$, ****$p<0.0001$, ns not significant.

829

830

831 **Figure S3. Distinct SFB isolates conferred reduced IAV levels and prevented IAV-induced**
832 **changes in lung cellularity, Related to Figure 4.**

833 **(A) (i) Experimental schema:** SFB^- mice were colonized with different SFB strain isolated from
834 the US, Japan, and France laboratories. Seven post colonization, mice were either inoculated or
835 not with CA09. On day 4.5 post virus inoculation, lungs were harvested to determine viral titer,
836 and feces were collected to determine SFB colonization level by qRT-PCR. Clinical signs were
837 monitored throughout the experiments. **(ii)** qRT-PCR analysis of SFB level from fecal samples.
838 **(iii)** Viral genome copies assayed by qRT-PCR, body weight, and temperatures. **(iv)** FACs
839 graphical representation, frequencies, and cell numbers of lung alveolar macrophages. **(v)** Cell
840 numbers of indicated immune cells.

841 All experiments n = 5 per group. Statistical analysis: SFB genomes, viral RN copies,
842 frequencies/cell numbers of immune cells data: One-way ANOVA. Body weight, temperature:
843 Two-way ANOVA. *$p<0.05$, **$p<0.01$, ***$p<0.001$, ****$p<0.0001$.

844

845 **Figure S4. SFB colonization diminished lung viral burden following inoculation of RSV or**
846 **SARS-CoV-2, Related to Figure 4.**

847 **(A)** SFB$^-$ mice were colonized with SFB for seven days before RSV inoculation. On day 4.5 post
848 virus inoculation were, mice were euthanized, and lungs were harvested to determine lung viral
849 titer or innate immune cells. Clinical signs were monitored daily. **(i)** Lung viral titer, body
850 weight, temperature. **(ii)** FACs graphical representation, frequencies, and cell numbers of lung
851 AMs. **(iii)** Frequencies and cell numbers of indicated immune cells.

852 **(B)** SFB$^-$ mice were colonized with SFB for seven days before SARS-CoV-2 MA10 strain
853 inoculation. On day 2 post virus inoculation were, mice were euthanized, and lungs were
854 harvested to determine lung viral titer or survival of AMs by FACs or pro-inflammatory genes
855 by qRT-PCR. Clinical signs were monitored daily. **(i)** Lung viral titer, body weight, temperature.
856 **(ii)** FACs graphical representation, frequencies, and cell numbers of lung AMs. **(iii)** Expression
857 of indicated pro-inflammatory genes.

858 All experiments n = 5 per group. Statistical analysis: viral titer, qRT-PCR data: student *t* test.
859 Frequencies/cell numbers of immune cells data: One-way ANOVA. Body weight, temperature:
860 Two-way ANOVA. *$p<0.05$, **$p<0.01$, ***$p<0.001$, ****$p<0.0001$.

861

862 **Figure S5. SFB prevented IAV infection of airway epithelial cells, Related to Figure 4.**

863 **(A)** Gating strategy for identification of airway epithelial cells and airway epithelial cells-
864 containing virus.

865 **(B)** SFB^- mice were colonized with SFB for seven days before CA09 inoculation. FACs
866 graphical representation, and frequencies of T1AECs-, T2AECs-, and conducting AECs-
867 containing CA09.

868 All experiments n = 5 per group. Data is representative of independent experiments, yielding an
869 identical pattern of results. Statistical analysis: One-way ANOVA. ****$p<0.0001$

870

871 **Figure S6. Colonization of intestine with SFB altered AM in ex vivo assays. Related to**
872 **Figure 6.**

873 **(A)** Biologic replication and qRT-PCR confirmation of SFB's impacts on basal AM gene
874 expression of RNA-seq from Figure 6B. qRT-PCR results of gene expression related to M2-like
875 macrophages, antiviral related genes, inflammation related genes, and other genes that
876 differentially express by lung AMs in the presence of SFB.

877 **(B)** SFB^- mice were colonized with SFB for seven days. Lungs were harvested and subjected to
878 FACs analysis for M1-like, and M2-like AMs. FACs graphical representation, and mean
879 fluorescence intensity of M1-like markers, and M2-like markers.

880

881 **(C)** C1qa are important for SFB mediated protection against influenza infection. AMs were
882 FACs sorted from $C1qa^{+/+}$ and $C1qa^{-/-}$ and some AMs from $C1qa^{+/+}$ mice were treated with C1qa
883 pAb and exposed to CA09 for 45mins and supernatant were collected. Virus infection titers in
884 supernatant were assayed by $TCID_{50}$ method.

885 **(D)** AMs from SFB^- and SFB^+ mice were FACs sorted and incubated for 18 hours at 37^0C. Cells
886 were then washed twice with serum-free media and incubated with live CA09 for 45 minutes and
887 supernatant were collected and CA09 genomes in supernatant were determined.

888 **(E)** SFB moderately enhanced AM uptake of fluorescent beads. AMs were sorted (D) and
889 incubated with fluorescent beads for two hours. FACs graphical representation and percentage of
890 AMs containing fluorescent beads.

891 **(F)** AMs were sorted and incubated as in (D), and where indicated, endocytosis/phagocytosis
892 inhibitors, chlorpromazine and latrunculin A (LatA) were added 10 minutes prior to addition of
893 CA09. Frequencies of live AMs after being treated with **(i)** chlorpromazine **(ii)** LatA). **(iii)** CA09
894 genomes in AM lysates.

895 All experiments in (A,B,D,E) at least n = 5 mice per group. Experiments were done in triplicate
896 (C). Data is representative of independent experiments, yielding an identical pattern of results
897 (A, B, D). Statistical analysis: MFI, and RT-qPCR of proinflammatory genes: student *t* test.
898 Vviral titer, CA09 RNA copies, %AM containing fluorescence beads data: One-way ANOVA.
899 *$p<0.05$, **$p<0.01$, ***$p<0.001$, ns not significant.

900

Figure S7. Antibody-mediated blockage of Notch4 partially recapitulated of SFB$^+$AM phenotypes ex vivo and in vivo, Related to Figure 6 and Figure 7.

(A) As schematized, AM was isolated from SFB$^-$ and SFB$^+$ mice and treated with UV-inactivated CA09 in the presence/absence of anti-Notch4 monoclonal antibodies. qRT-PCR results of *Il6,* and type I interferon-related genes from AM.

(B) **(i)** As schematized, CD45.1 SFB$^-$ mice were administered SFB or PBS. Seven days later, AMs were isolated by FACs. Some SFB$^-$ AM were then treated with an anti-Notch4 monoclonal antibody or isotype. AM were then transferred to CD45.2 SFB$^-$ mice, $5x10^5$ per mouse. One day post transfer, mice were inoculated with CA09. Mice were euthanized on day 4.5 post virus inoculation. FACs graphical representation, frequencies, and cell numbers of endogenous and exogenous AM. **(ii)** lung CA09 viral genomes copies, survival rate and body weight. **(iii)** FACs graphical representation and frequencies of AECs-containing CA09.

All experiments n =5 mice per group. Data is representative of two independent experiments, yielding an identical pattern of results. Statistical test: Relative expression of pro-inflammatory genes, CA09 RNA copies, frequencies of GFP+ cells data: one-way ANOVA. Survival data; one-way ANOVA. Body weight: Two-way ANOVA *$p<0.05$, **$p<0.01$, ***$p<0.001$, ****$p<0.0001$, ns not significant.

Figure 1

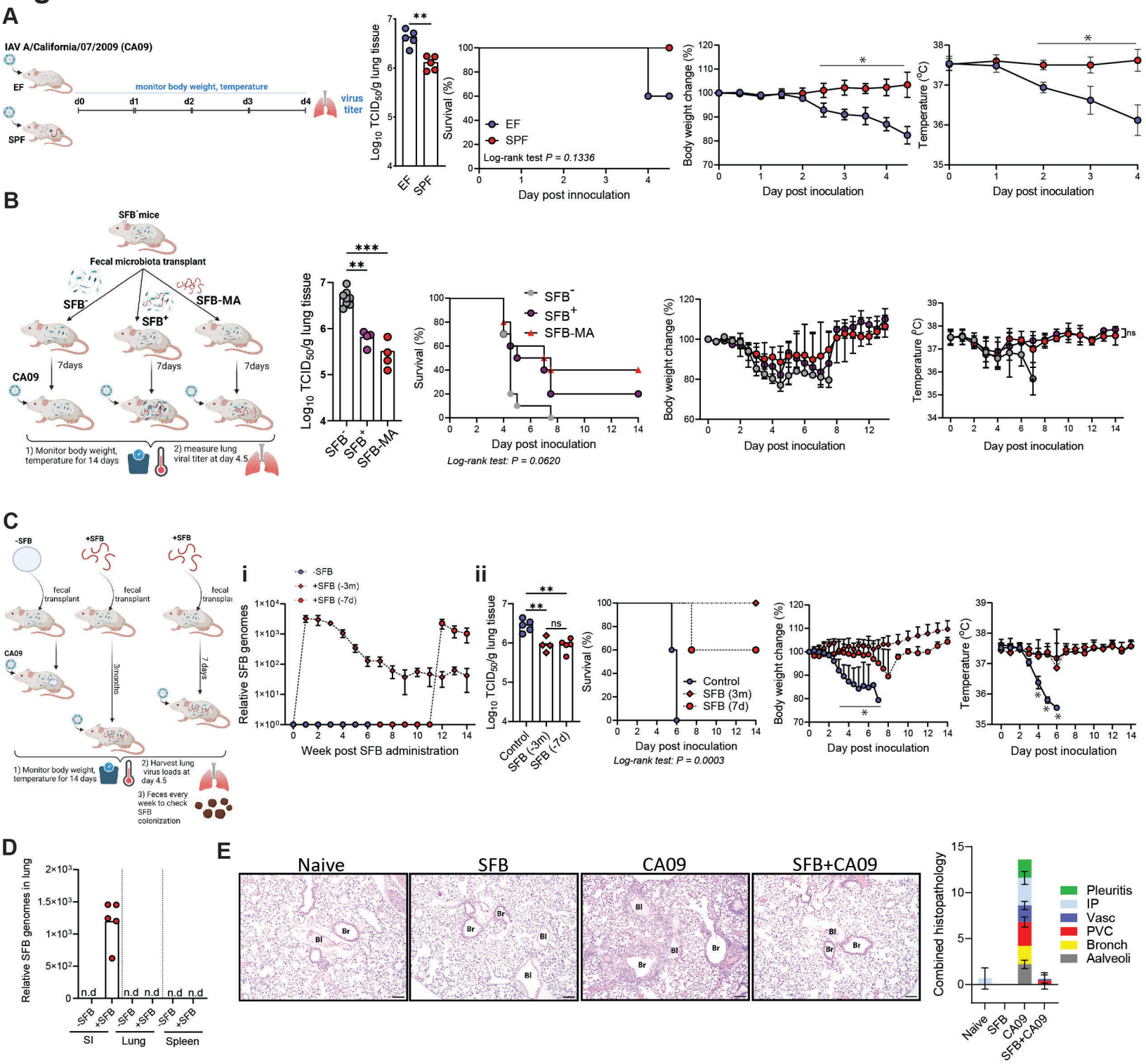
A
IAV A/California/07/2009 (CA09)
EF
SPF
monitor body weight, temperature
d0
d1
d2
d3
d4
virus titer
Log10 TCID50/g lung tissue
Survival (%)
Log-rank test P = 0.1336
Day post innoculation
Body weight change (%)
Temperature (°C)
Day post inoculation
B
SFB⁻mice
Fecal microbiota transplant
SFB⁻
SFB⁺
SFB-MA
7days
CA09
1) Monitor body weight, temperature for 14 days
2) measure lung viral titer at day 4.5
Log-rank test: P = 0.0620
C
-SFB
+SFB
fecal transplant
3months
7days
1) Monitor body weight, temperature for 14 days
2) Harvest lung virus loads at day 4.5
3) Feces every week to check SFB colonization
Relative SFB genomes
Week post SFB administration
+SFB (-3m)
+SFB (-7d)
Control
SFB (-3m)
SFB (-7d)
Log-rank test: P = 0.0003
D
Relative SFB genomes in lung
n.d
SI
Lung
Spleen
E
Naive
SFB
CA09
SFB+CA09
Br
Bl
Combined histopathology
Pleuritis
IP
Vasc
PVC
Bronch
Aalveoli

Figure 2

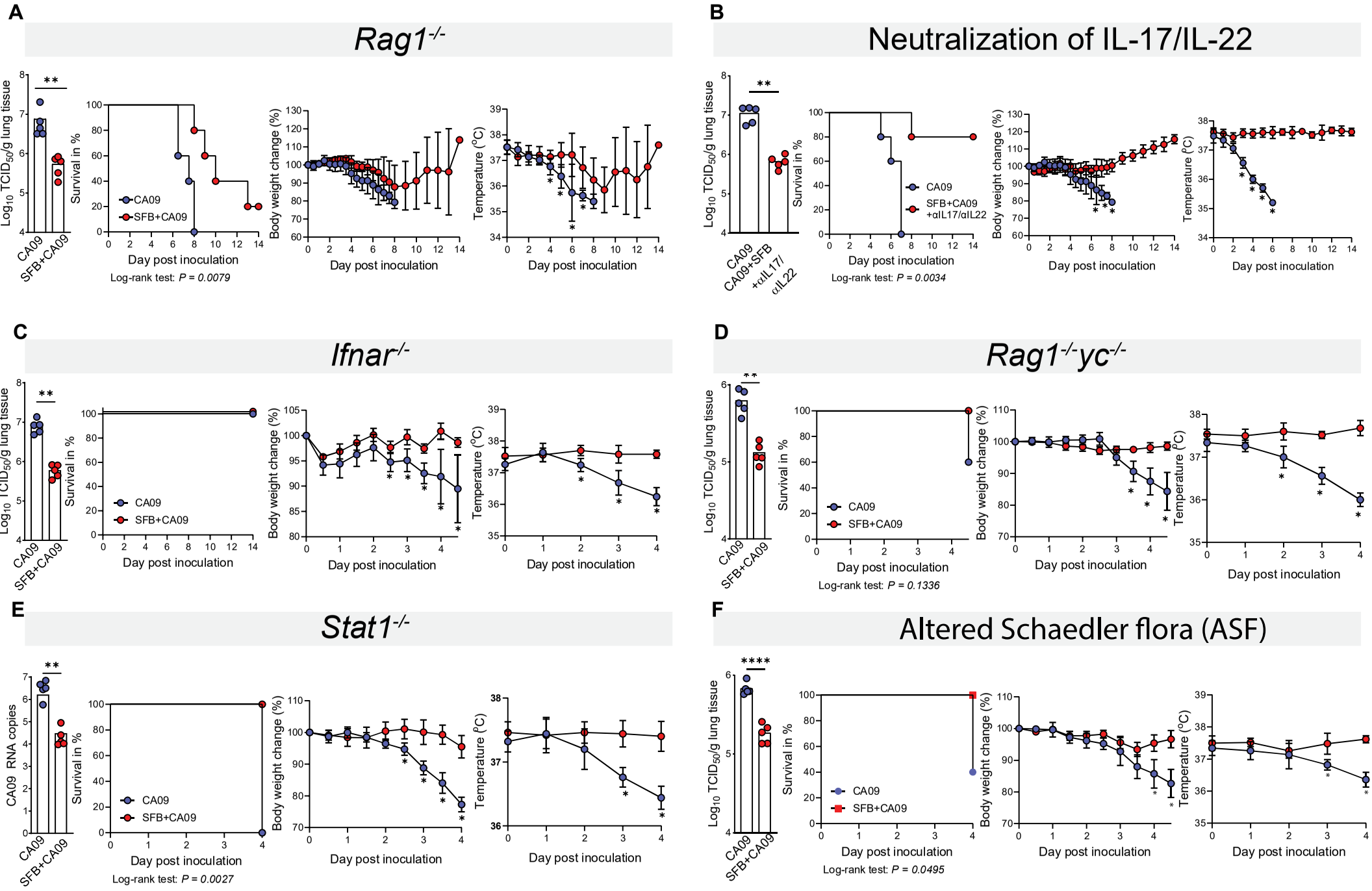
A
Rag1-/-
B
Neutralization of IL-17/IL-22
C
Ifnar-/-
D
Rag1-/-yc-/-
E
Stat1-/-
F
Altered Schaedler flora (ASF)
Log10 TCID50/g lung tissue
CA09 RNA copies
Survival in %
Body weight change (%)
Temperature (°C)
Day post inoculation
CA09
SFB+CA09
CA09+SFB +αIL17/ αIL22
SFB+CA09 +αIL17/αIL22
Log-rank test: P = 0.0079
Log-rank test: P = 0.0034
Log-rank test: P = 0.1336
Log-rank test: P = 0.0027
Log-rank test: P = 0.0495
**
****

Figure 3

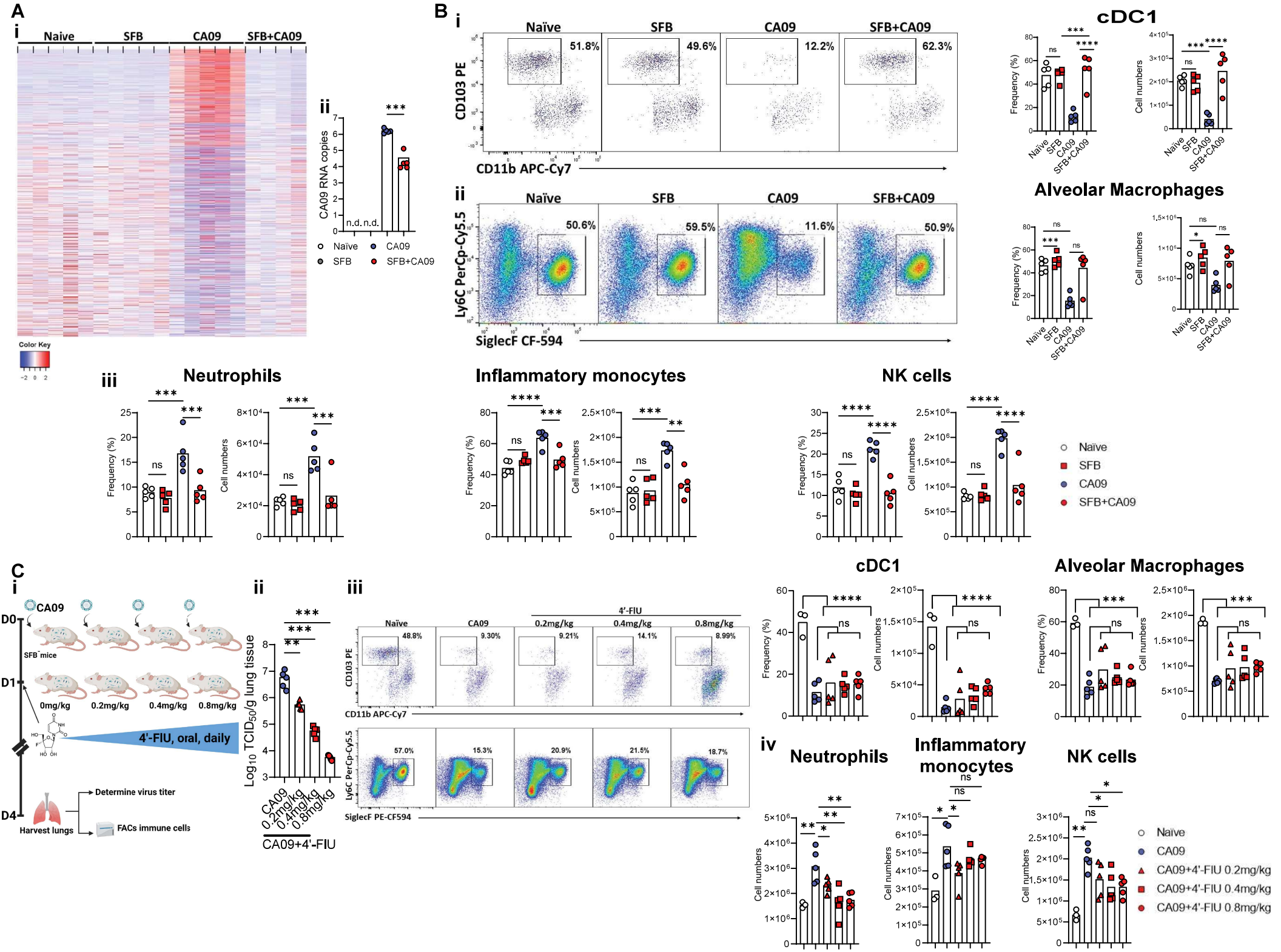
A
i
Naive
SFB
CA09
SFB+CA09
Color Key
ii
CA09 RNA copies
n.d. n.d.
Naïve
SFB
CA09
SFB+CA09
B
i
Naïve
SFB
CA09
SFB+CA09
51.8%
49.6%
12.2%
62.3%
CD103 PE
CD11b APC-Cy7
cDC1
Frequency (%)
Cell numbers
ii
50.6%
59.5%
11.6%
50.9%
Ly6C PerCp-Cy5.5
SiglecF CF-594
Alveolar Macrophages
iii
Neutrophils
Inflammatory monocytes
NK cells
Naïve
SFB
CA09
SFB+CA09
C
i
CA09
D0
SFB mice
D1
0mg/kg
0.2mg/kg
0.4mg/kg
0.8mg/kg
4'-FIU, oral, daily
D4
Harvest lungs
Determine virus titer
FACs immune cells
ii
Log10 TCID50/g lung tissue
CA09
0.2mg/kg
0.4mg/kg
0.8mg/kg
CA09+4'-FIU
iii
4'-FIU
Naïve
CA09
0.2mg/kg
0.4mg/kg
0.8mg/kg
48.8%
9.30%
9.21%
14.1%
8.99%
CD103 PE
CD11b APC-Cy7
57.0%
15.3%
20.9%
21.5%
18.7%
Ly6C PerCp-Cy5.5
SiglecF PE-CF594
cDC1
Alveolar Macrophages
iv
Neutrophils
Inflammatory monocytes
NK cells
Naive
CA09
CA09+4'-FIU 0.2mg/kg
CA09+4'-FIU 0.4mg/kg
CA09+4'-FIU 0.8mg/kg

Figure 4

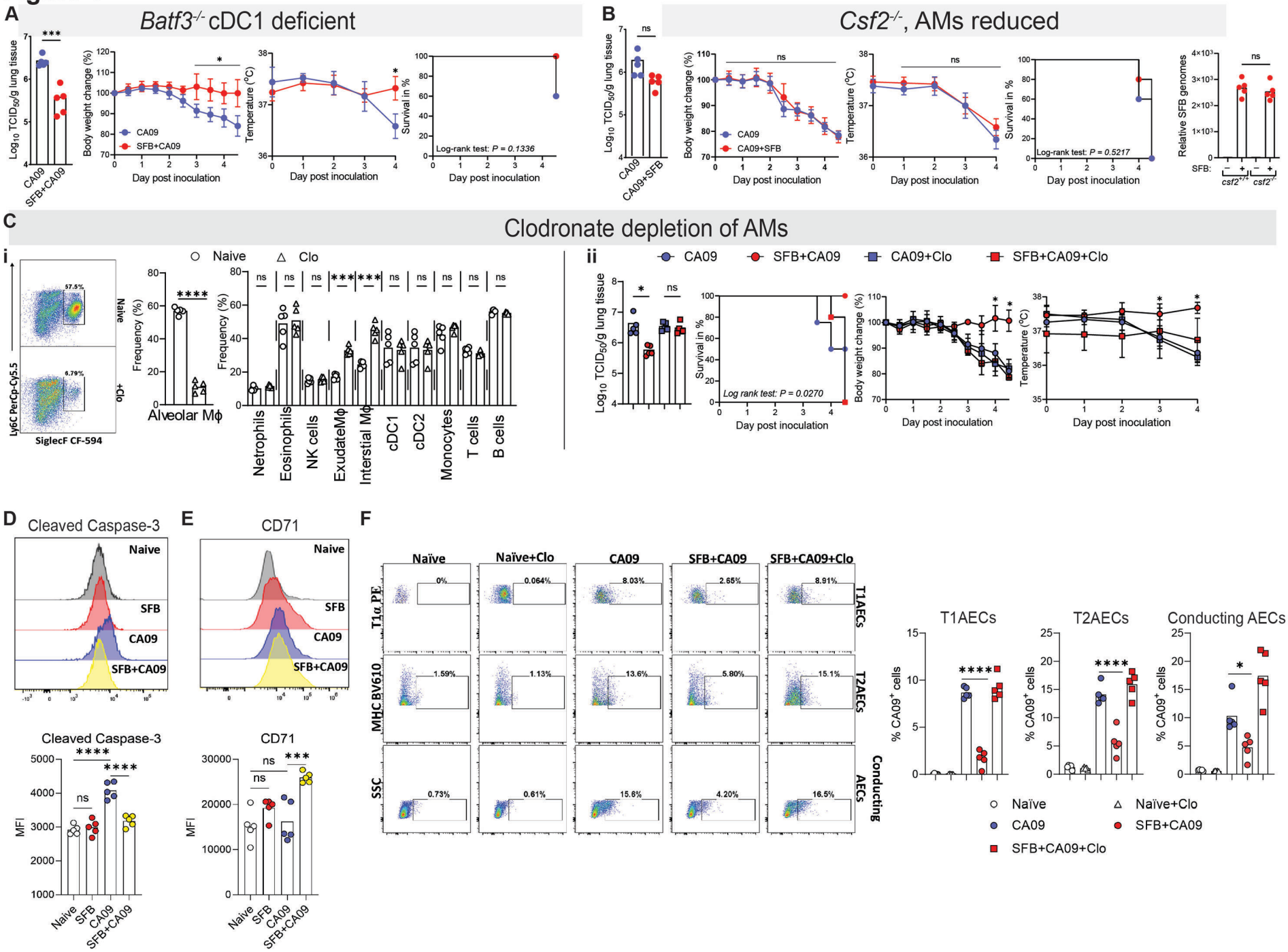
A
Batf3-/- cDC1 deficient
Log10 TCID50/g lung tissue
CA09
SFB+CA09
Body weight change (%)
Day post inoculation
Temperature (°C)
Survival in %
Log-rank test: P = 0.1336
B
Csf2-/-, AMs reduced
CA09+SFB
Log-rank test: P = 0.5217
Relative SFB genomes
SFB:
csf2+/+
csf2-/-
C
Clodronate depletion of AMs
i
Naive
Clo
Ly6C PerCp-Cy5.5
SiglecF CF-594
57.5%
6.79%
Frequency (%)
Alveolar Mϕ
Netrophils
Eosinophils
NK cells
ExudateMϕ
Interstial Mϕ
cDC1
cDC2
Monocytes
T cells
B cells
ii
CA09+Clo
SFB+CA09+Clo
Log rank test: P = 0.0270
D
Cleaved Caspase-3
MFI
E
CD71
F
Naïve
Naïve+Clo
T1α PE
MHC BV610
SSC
T1AECs
T2AECs
Conducting AECs
% CA09+ cells

Figure 5

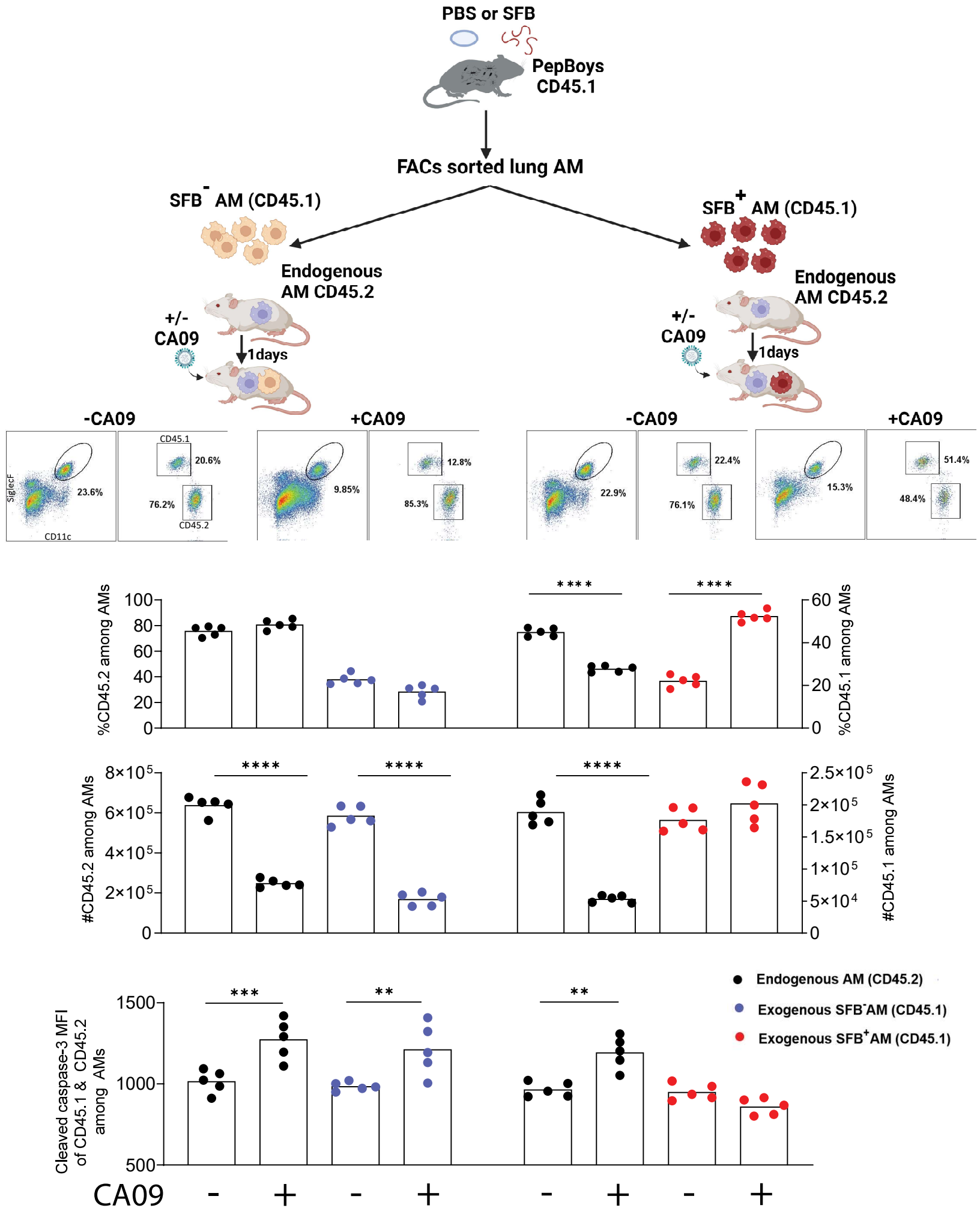
PBS or SFB
PepBoys CD45.1
FACs sorted lung AM
SFB- AM (CD45.1)
SFB+ AM (CD45.1)
Endogenous AM CD45.2
+/- CA09
1days
-CA09
+CA09
SiglecF
CD11c
CD45.1
CD45.2
23.6%
20.6%
76.2%
9.85%
12.8%
85.3%
22.9%
22.4%
76.1%
15.3%
51.4%
48.4%
%CD45.2 among AMs
%CD45.1 among AMs
#CD45.2 among AMs
#CD45.1 among AMs
Cleaved caspase-3 MFI of CD45.1 & CD45.2 among AMs
Endogenous AM (CD45.2)
Exogenous SFB-AM (CD45.1)
Exogenous SFB+AM (CD45.1)
CA09

Figure 6

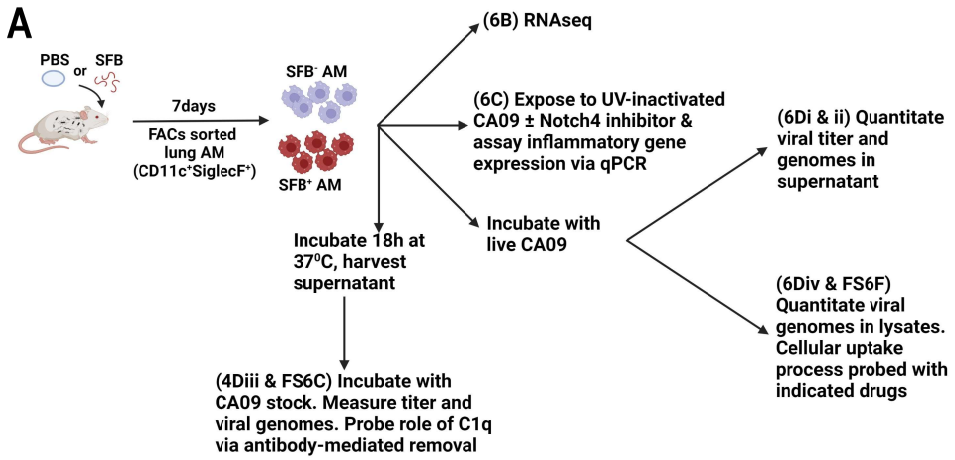
A
PBS or SFB
7days
FACs sorted lung AM (CD11c+SiglecF+)
SFB- AM
SFB+ AM
(6B) RNAseq
(6C) Expose to UV-inactivated CA09 ± Notch4 inhibitor & assay inflammatory gene expression via qPCR
Incubate with live CA09
(6Di & ii) Quantitate viral titer and genomes in supernatant
(6Div & FS6F) Quantitate viral genomes in lysates. Cellular uptake process probed with indicated drugs
Incubate 18h at 37°C, harvest supernatant
(4Diii & FS6C) Incubate with CA09 stock. Measure titer and viral genomes. Probe role of C1q via antibody-mediated removal

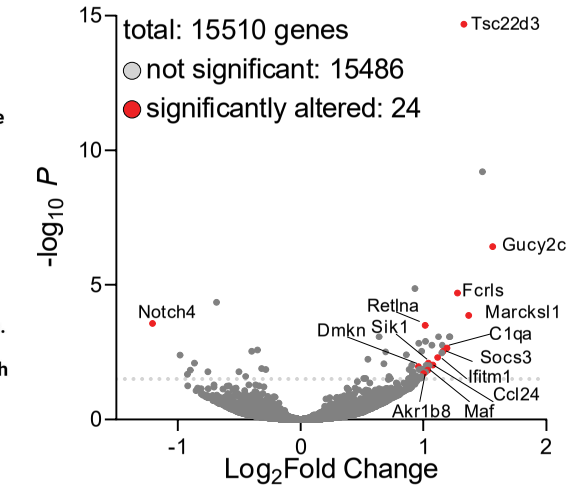
B
total: 15510 genes
not significant: 15486
significantly altered: 24
-log10 P
Log2Fold Change
Tsc22d3
Gucy2c
Fcrls
Marcksl1
C1qa
Socs3
Ifitm1
Ccl24
Maf
Akr1b8
Retlna
Dmkn
Sik1
Notch4

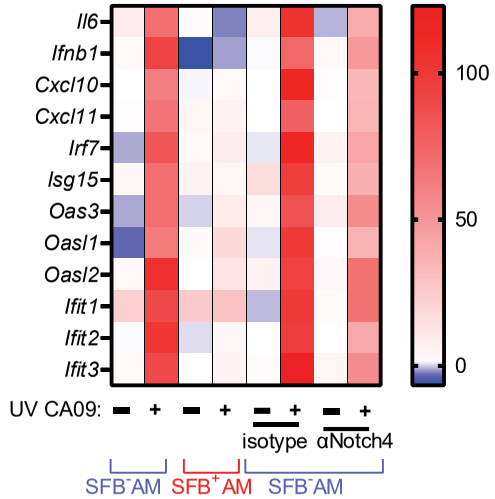
C
Il6
Ifnb1
Cxcl10
Cxcl11
Irf7
Isg15
Oas3
Oasl1
Oasl2
Ifit1
Ifit2
Ifit3
UV CA09:
isotype
αNotch4
SFB-AM
SFB+AM
SFB-AM
100
50
0

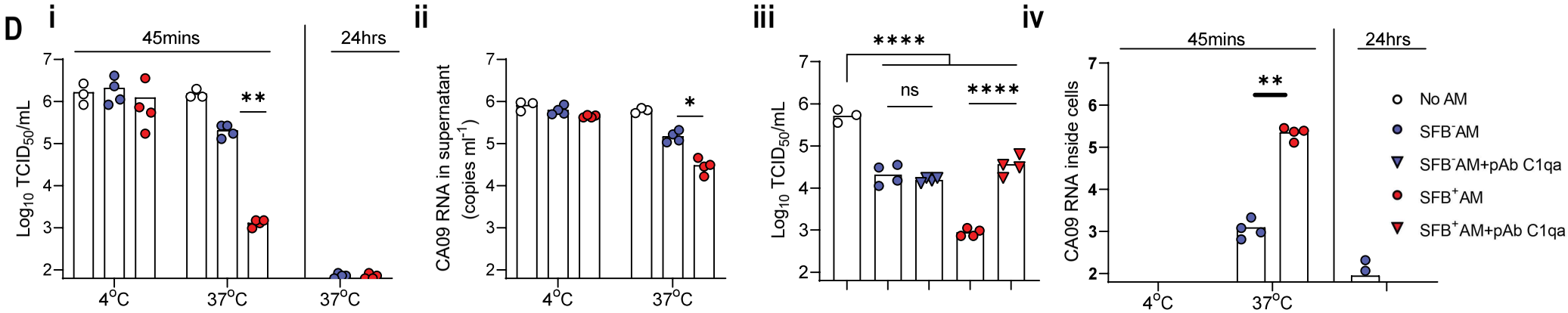
D
i
45mins
24hrs
Log10 TCID50/mL
4°C
37°C
37°C
ii
CA09 RNA in supernatant (copies ml-1)
4°C
37°C
iii
Log10 TCID50/mL
ns
iv
CA09 RNA inside cells
4°C
37°C
No AM
SFB-AM
SFB-AM+pAb C1qa
SFB+AM
SFB+AM+pAb C1qa

Figure 7

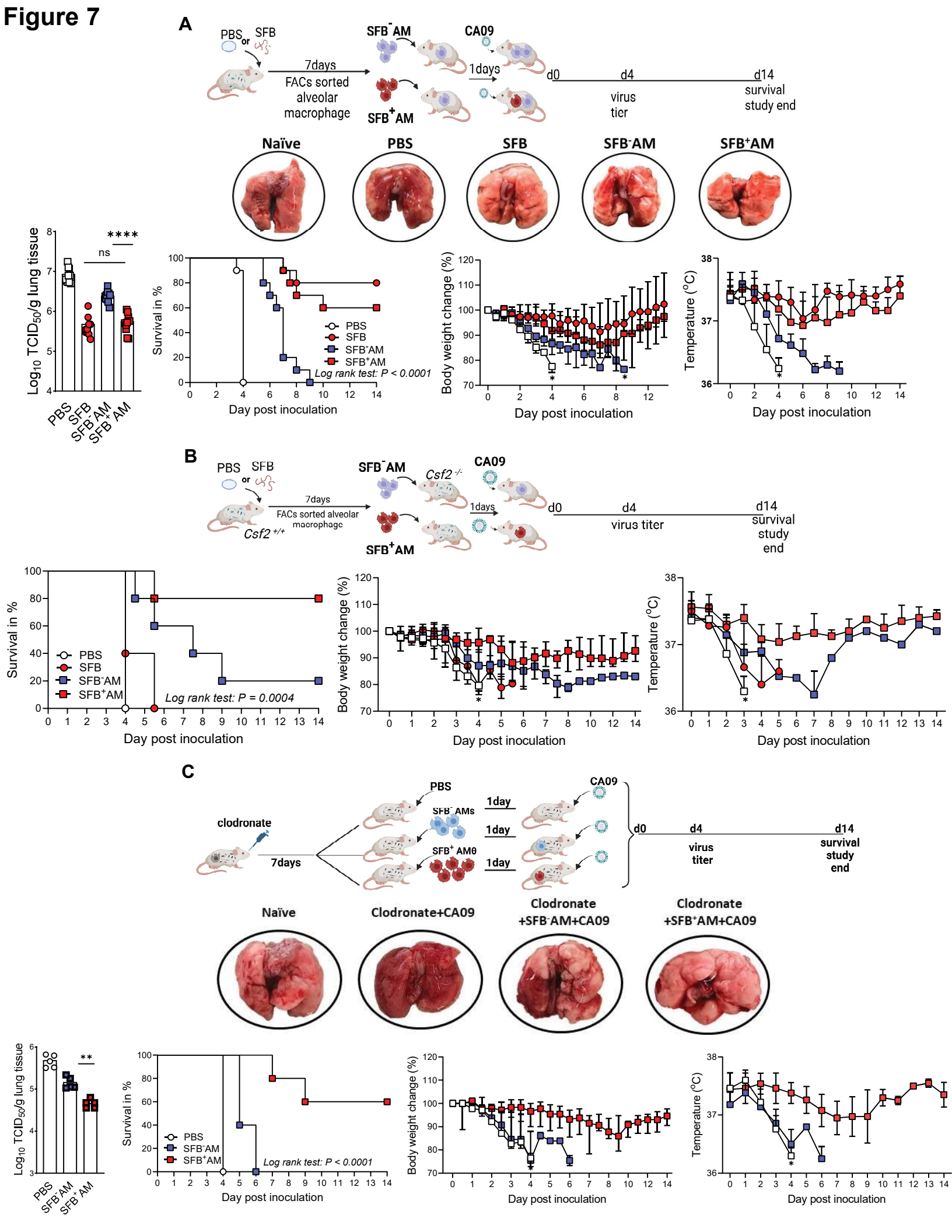
A
PBS or SFB
7days
FACs sorted alveolar macrophage
SFB⁻AM
SFB⁺AM
CA09
1days
d0
d4
virus tier
d14
survival study end
Naïve
PBS
SFB
SFB⁻AM
SFB⁺AM
Log10 TCID50/g lung tissue
****
ns
PBS
SFB
SFB⁻AM
SFB⁺AM
Survival in %
Log rank test: P < 0.0001
Day post inoculation
Body weight change (%)
Temperature (°C)
B
Csf2 +/+
Csf2 -/-
Log rank test: P = 0.0004
C
clodronate
7days
PBS
SFB⁻AMs
SFB⁺ AMθ
1day
CA09
Naïve
Clodronate+CA09
Clodronate +SFB⁻AM+CA09
Clodronate +SFB⁺AM+CA09
**

Figure S1 (related to F1)

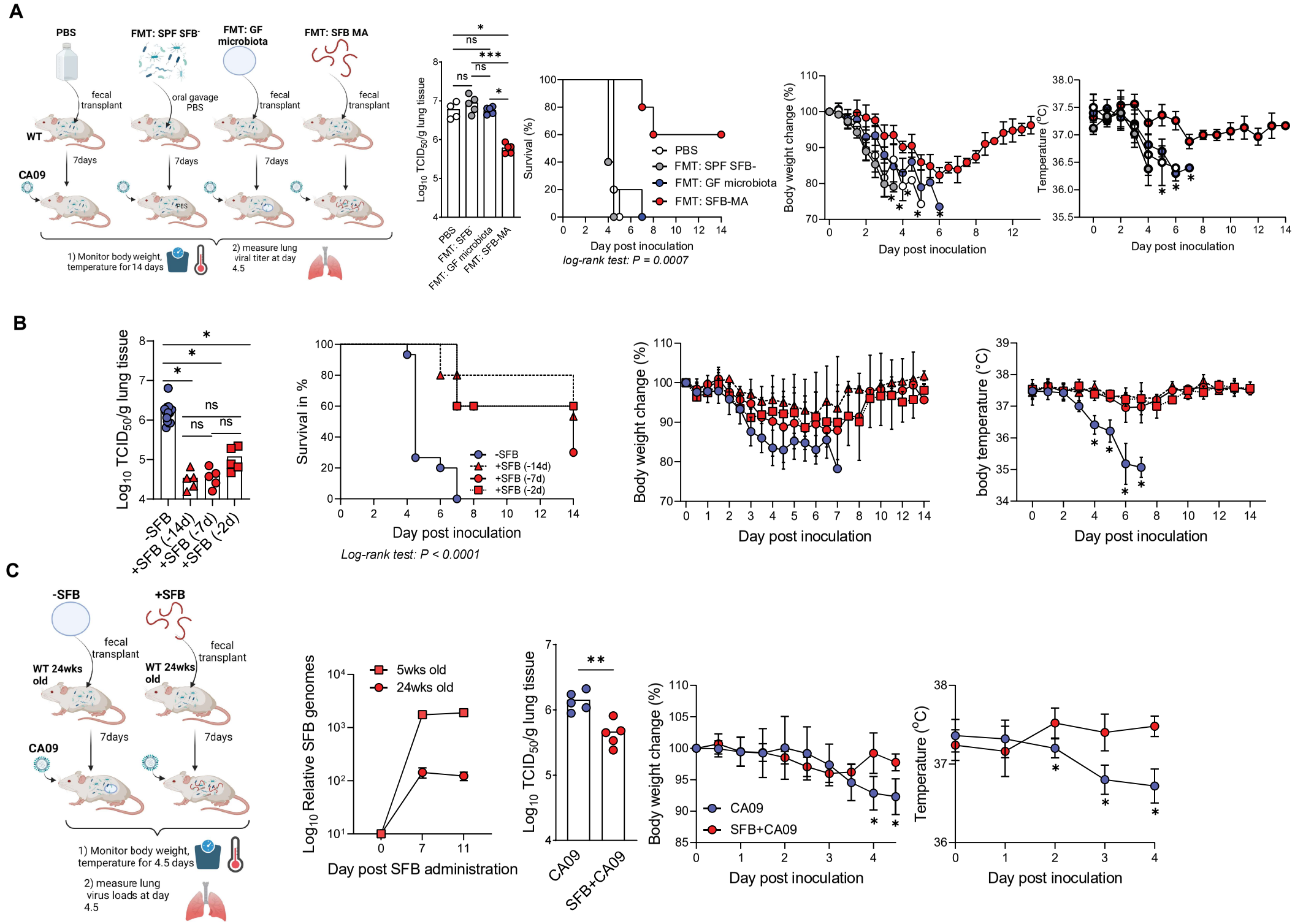

Figure S2 (related to F3)

A

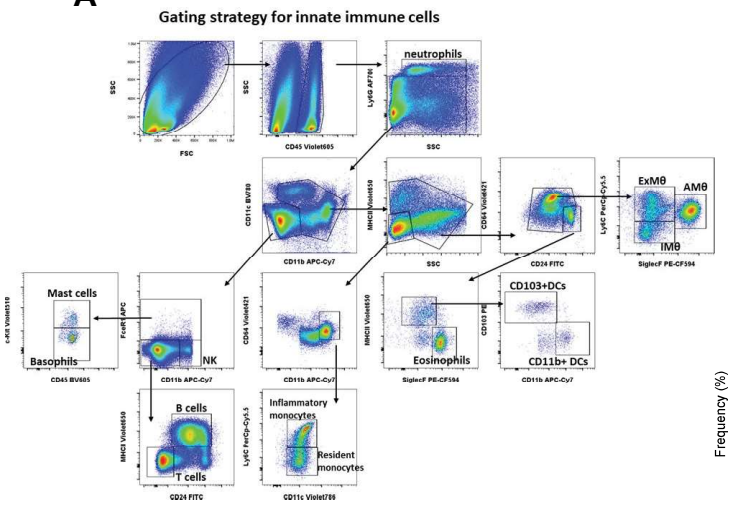

B

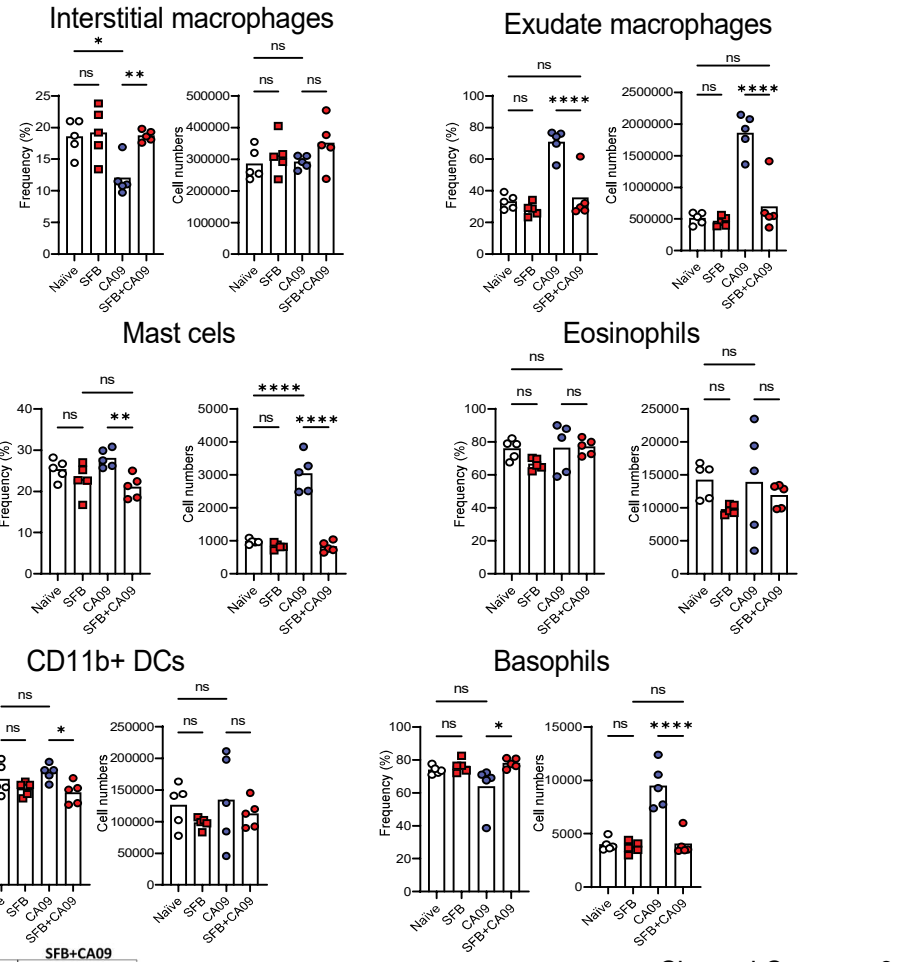

C

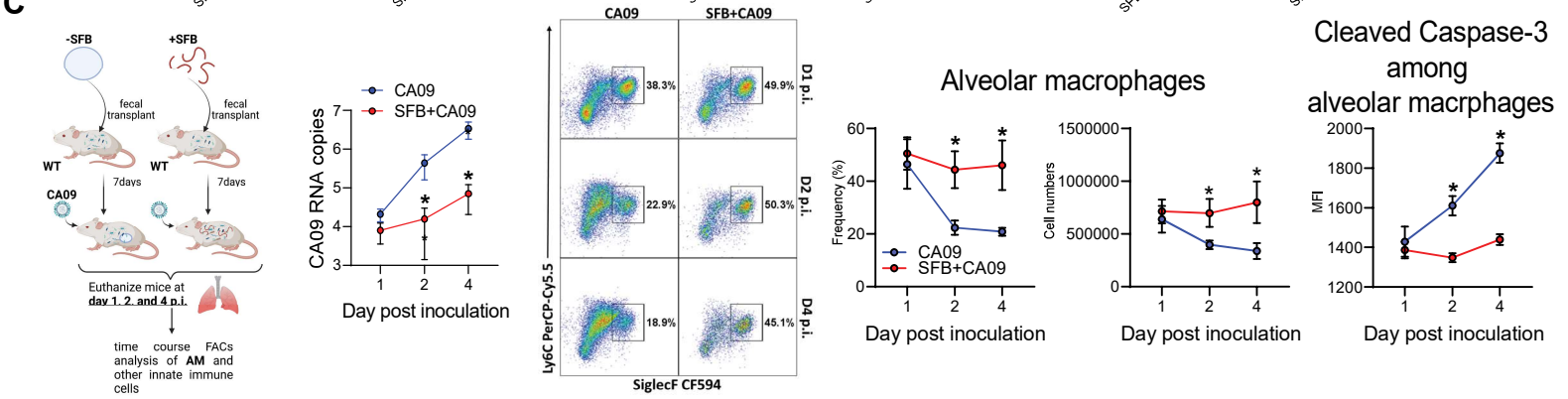

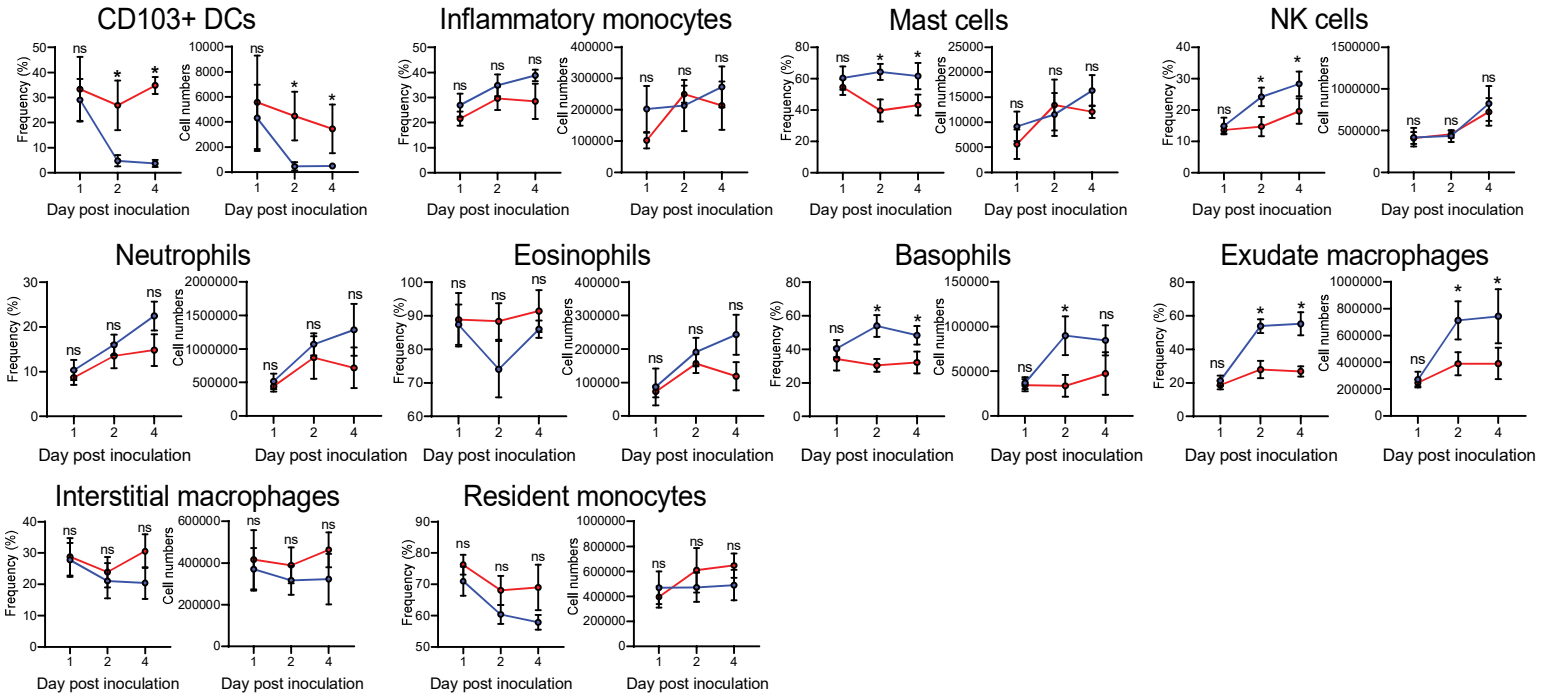

Figure S3 (related to F4)

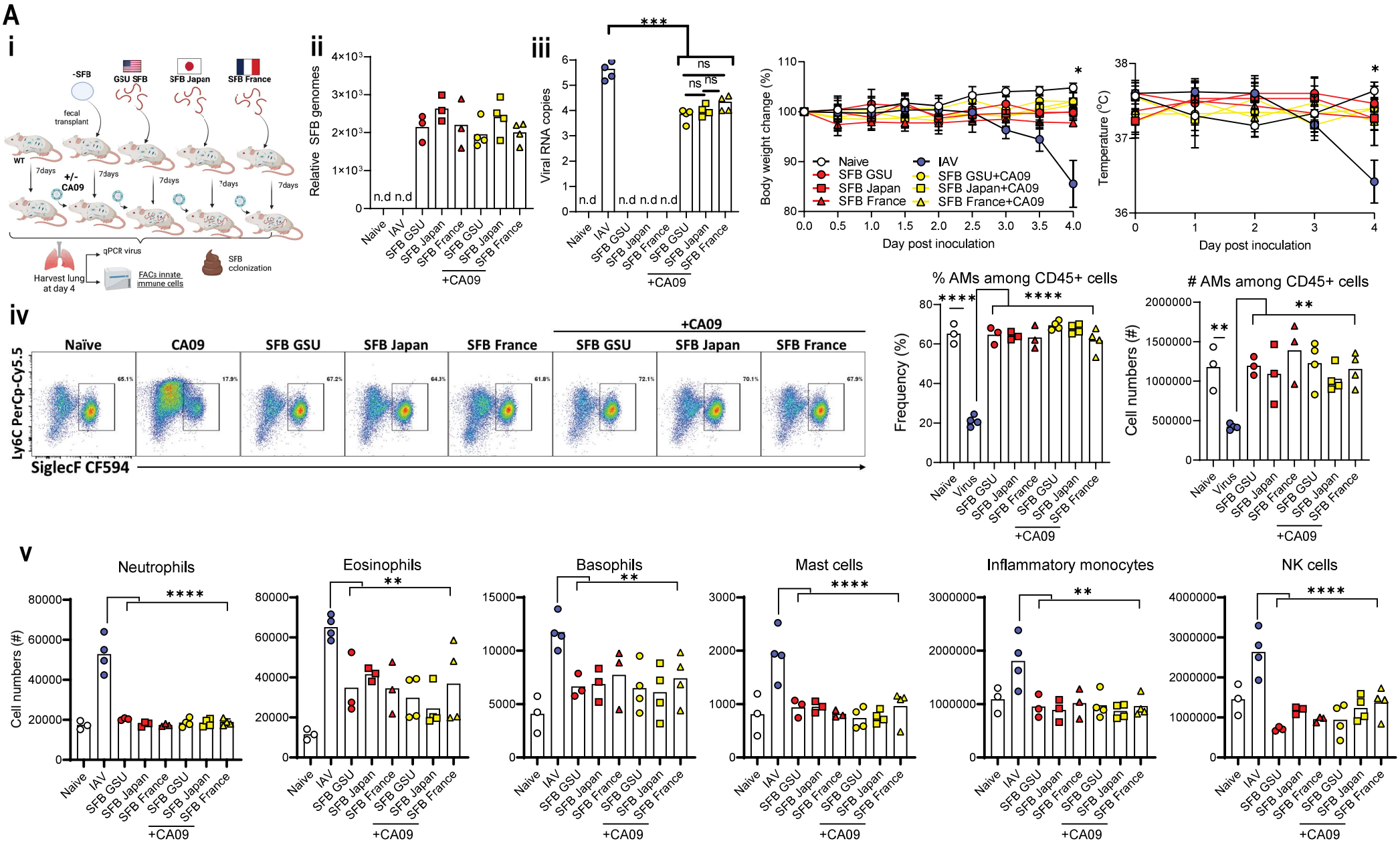

Figure S4 (related to F4)

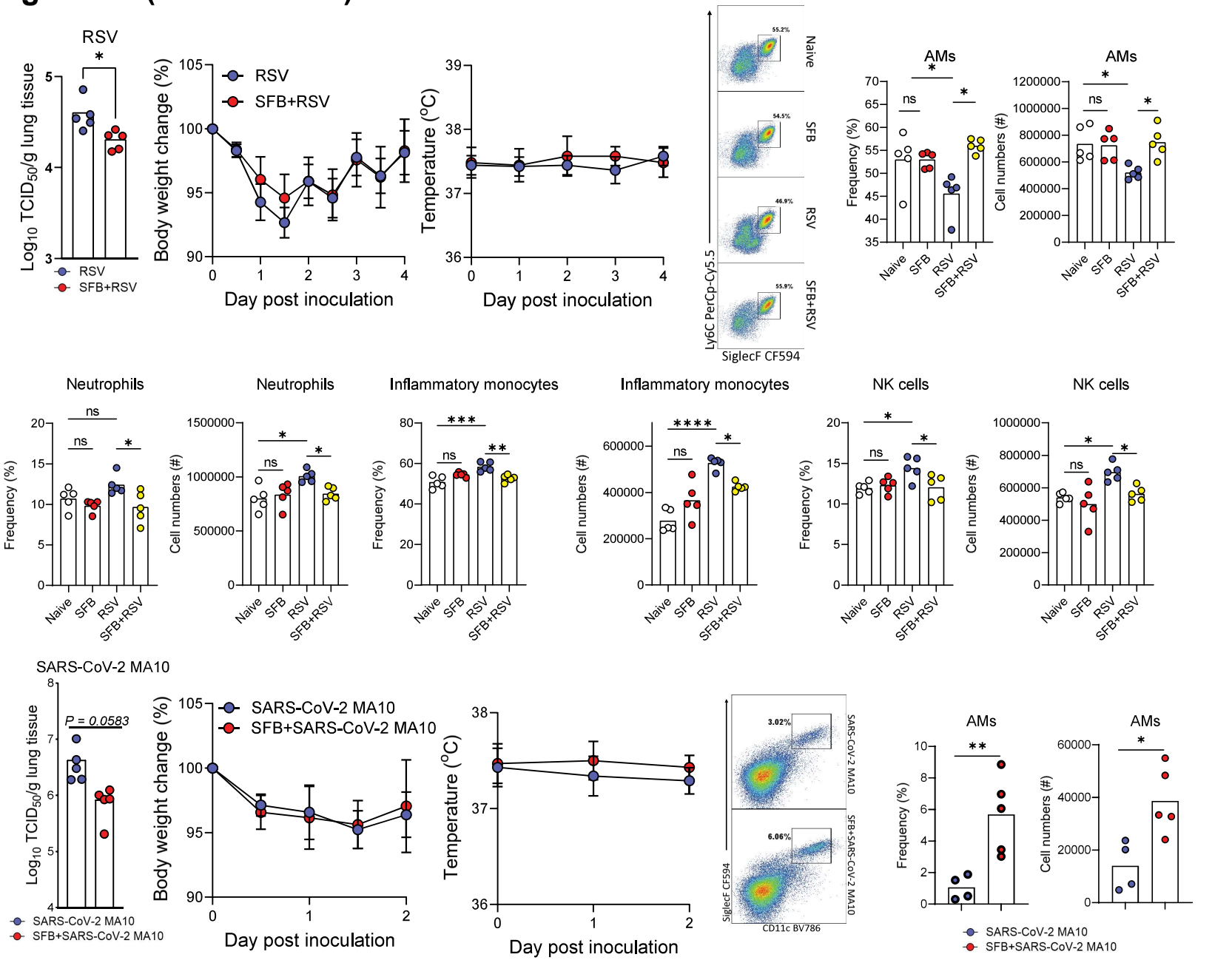

Figure S5 (related to F4)

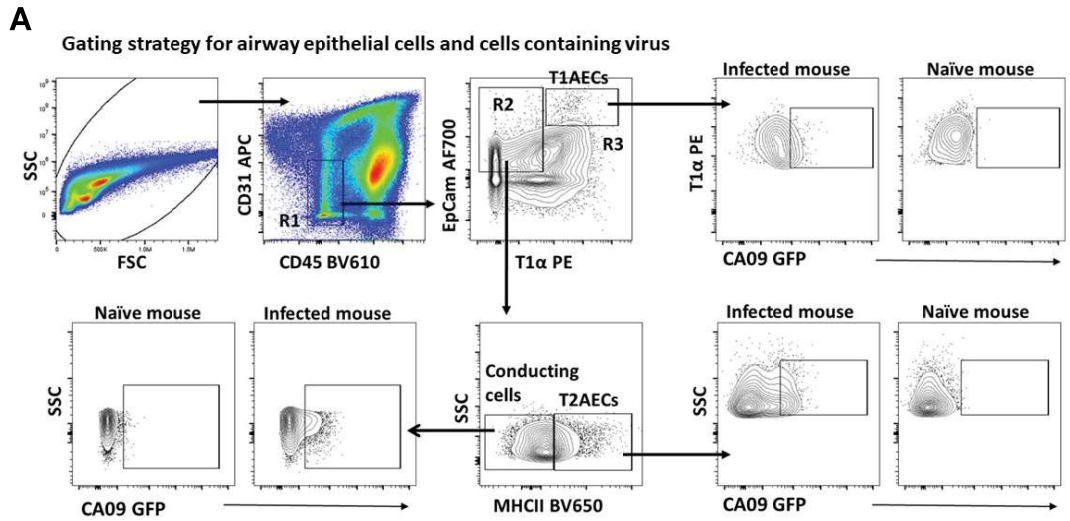

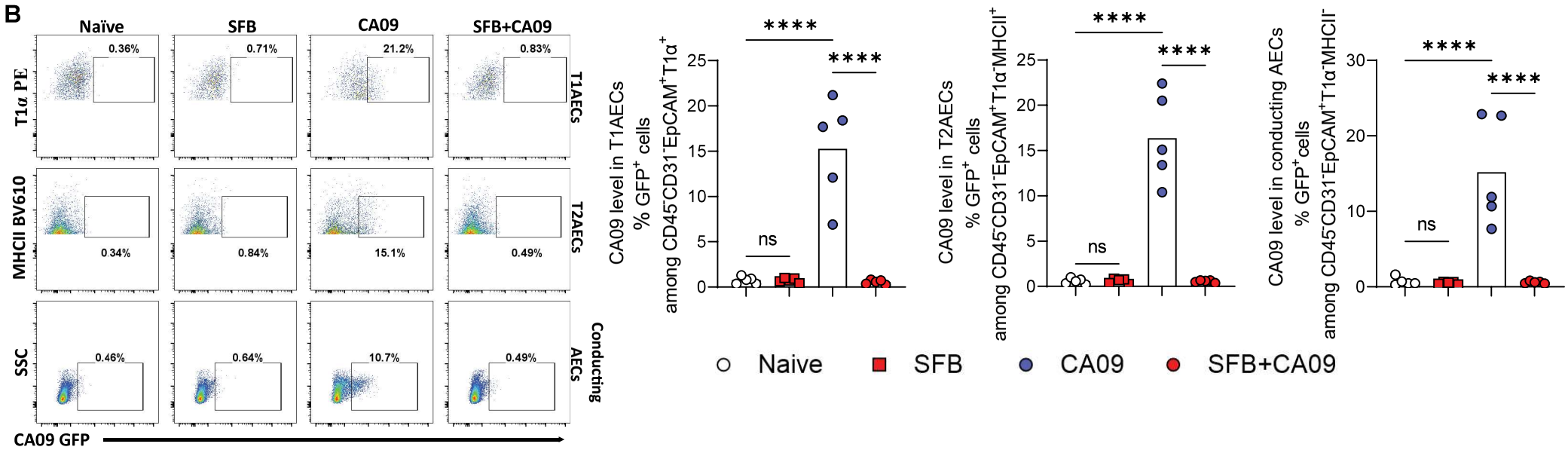

Figure S6 (related to Fig 6)

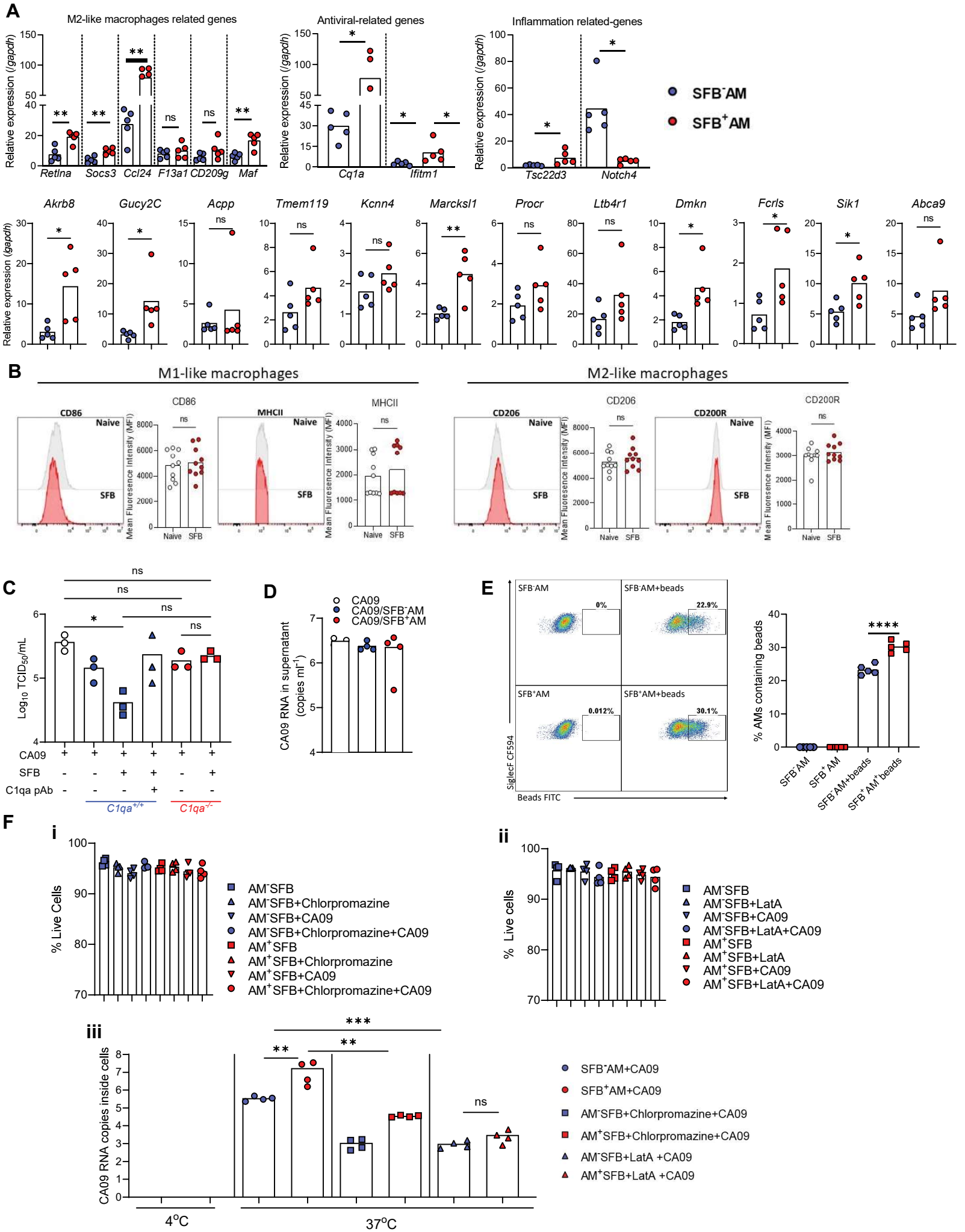
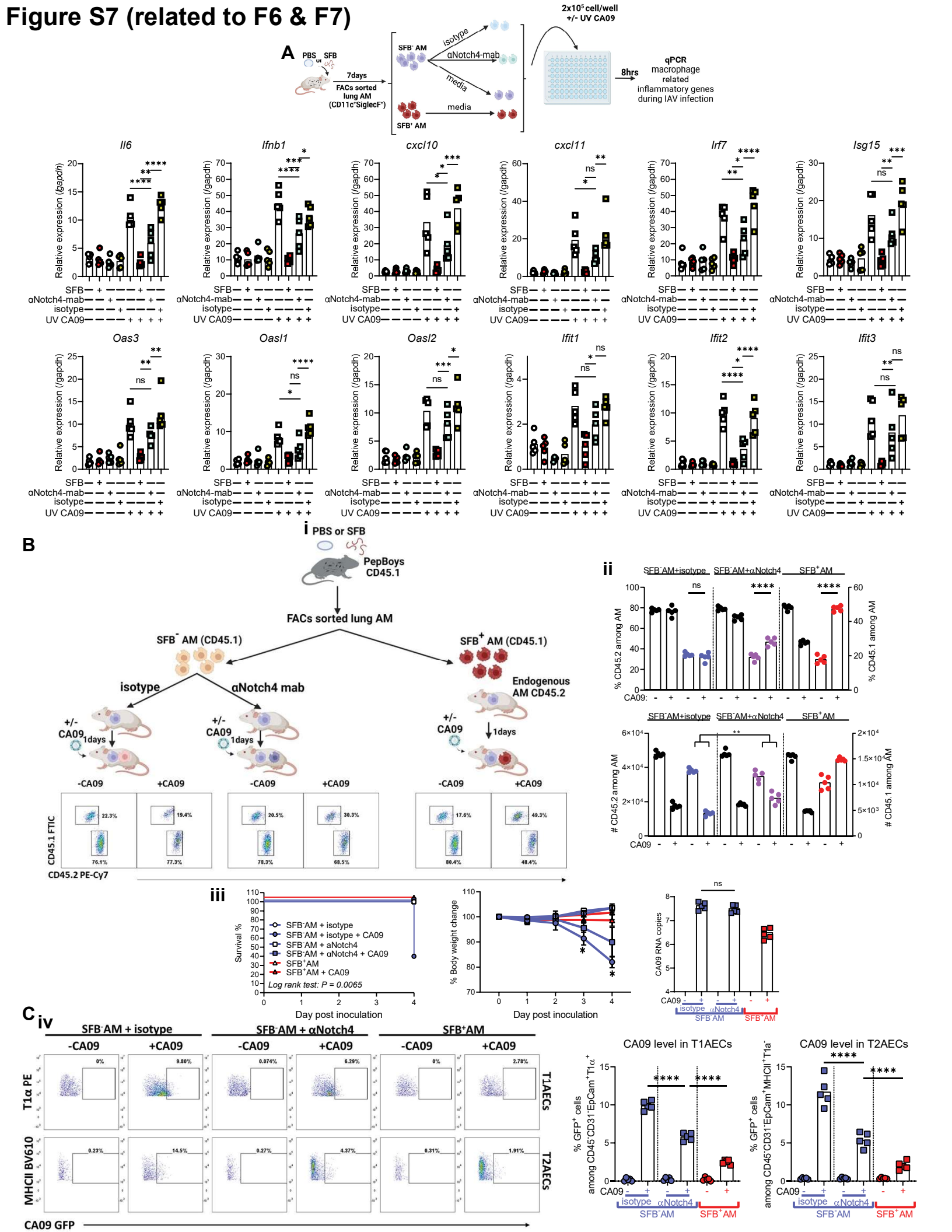
Figure S7 (related to F6 & F7)